Agricultural Water Management 287 (2023) 108422

Contents lists available at ScienceDirect

Agricultural Water Management

journal homepage: www.elsevier.com/locate/agwat

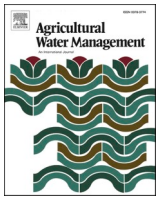

Evaluation of soil moisture estimation techniques based on Sentinel-1 observations over wheat fields

María Arias [a], Claudia Notarnicola [b], Miguel Ángel Campo-Bescós [a], Luis Miguel Arregui [c], Jesús Álvarez-Mozos [a,*]

[a] Institute for Sustainability & Food Chain Innovation (IS-FOOD), Department of Engineering, Public University of Navarre (UPNA), Arrosadia Campus, 31006 Pamplona, Spain
[b] Institute for Earth Observation, EURAC Research, Viale Druso, 1, 39100 Bolzano, Italy
[c] Institute for Sustainability & Food Chain Innovation (IS-FOOD), Department of Agricultural Engineering, Biotechnology and Food, Public University of Navarre (UPNA), Arrosadia Campus, 31006 Pamplona, Spain

ARTICLE INFO

Handling Editor - J.E. Fernández

Keywords:
Soil wetness
Agriculture
SAR
Change detection
Field scale

ABSTRACT

Soil moisture (SM) is a key variable in agriculture and its monitoring is essential. SM determines the amount of water available to plants, having a direct impact on the development of crops, on the forecasting of crop yields and on the surveillance of food security. Microwave remote sensing offers a great potential for estimating SM because it is sensitive to the dielectric characteristics of observed surface that depend on surface soil moisture. The objective of this study is the evaluation of three change detection methodologies for SM estimation over wheat at the agricultural field scale based on Sentinel-1 time series: Short Term Change Detection (STCD), TU Wien Change Detection (TUWCD) and Multitemporal Bayesian Change Detection (MTBCD). Different methodological alternatives were proposed for the implementation of these techniques at the agricultural field scale. Soil moisture measurements from eight experimental wheat fields were used for validating the methodologies. All available Sentinel-1 acquisitions were processed and the eventual benefit of correcting for vegetation effects in backscatter time series was evaluated. The results were rather variable, with some experimental fields achieving successful performance metrics (ubRMSE ~ 0.05 m^3/m^3) and some others rather poor ones (ubRMSE > 0.12 m^3/m^3). Evaluating median performance metrics, it was observed that both TUWCD and MTBCD methods obtained better results when run with vegetation corrected backscatter time series (ubRMSE ~0.07 m^3/m^3) whereas STCD produced similar results with and without vegetation correction (ubRMSE ~0.08 m^3/m^3). The soil moisture content had an influence on the accuracy of the different methodologies, with higher errors observed for drier conditions and rain-fed fields, in comparison to wetter conditions and irrigated fields. Taking into account the spatial scale of this case study, results were considered promising for the future application of these techniques in irrigation management.

1. Introduction

Soil moisture (SM) is a key variable for understanding, modeling and forecasting different processes occurring at the Earth surface (Brocca et al., 2018; Green et al., 2019; Liu et al., 2020; Seneviratne et al., 2010; Wasko and Nathan, 2019). Due to its relevance, in 2010 it was recognized as an Essential Climate Variable (ECV) by the Global Climate Observing System (GCOS) of the United Nations Framework Convention on Climate Change (UNFCCC). Its monitoring is therefore necessary to track our changing climate and design proper mitigation and adaptation measures. In agricultural systems, SM determines the amount of water available to plants, and therefore, it has a direct impact on the development of crops and on the forecasting of crop yields. Therefore, SM monitoring is essential for the surveillance of food security (Lobell and Burke, 2010).

Remote sensing has a great potential for SM retrieval due to its capability to observe large areas of the territory repeatedly over time. Although optical and thermal sensors have potential for SM estimation

* Correspondence to: Public University of Navarre, Department of Engineering, Los Tejos Building, Campus de Arrosadia, 31006 Pamplona, Spain.
E-mail addresses: maria.arias@unavarra.es (M. Arias), claudia.notarnicola@eurac.edu (C. Notarnicola), miguel.campo@unavarra.es (M.Á. Campo-Bescós), arregui@unavarra.es (L.M. Arregui), jesus.alvarez@unavarra.es (J. Álvarez-Mozos).

https://doi.org/10.1016/j.agwat.2023.108422
Received 28 April 2023; Received in revised form 9 June 2023; Accepted 17 June 2023
Available online 21 June 2023

(Verstraeten et al., 2006; Wang and Qu, 2007), most progress in the last decades has been achieved by the microwave scientific community (Entekhabi et al., 2010a; Kerr et al., 2001; Wagner et al., 1999), due to the long-time known sensitivity of microwave reflectance and emissivity to the dielectric characteristics of observed surfaces, which mostly depend on surface SM (Ulaby and Long, 2014).

In recent years, global SM products at coarse spatial resolution (10–50 km) have been developed, principally based on radiometers or scatterometers (Brocca et al., 2011; Chan et al., 2016; Kerr et al., 2012; Naeimi et al., 2009). Synthetic aperture radar (SAR) sensors achieve finer spatial resolutions (10–20 m) that might be suitable to work at the scale of agricultural fields. This possibility is very appealing as it would enable a field scale SM monitoring, with direct implications for irrigation management, harvest forecast and disease control. However, SM estimation at this scale is still challenging (Peng et al., 2021), because SAR sensors are also sensitive to other variables related to vegetation (Bindlish and Barros, 2001) or soil surface roughness (Verhoest et al., 2008). Therefore, the inversion of classic bare soil backscatter models, such as the physically based Integral Equation Model (IEM) (Fung, 1994) or the semi-empirical models of Oh et al. (1992), Dubois et al. (1995) or Shi et al. (1997), is generally ill-posed and its operational application not guaranteed. Moreover, SM estimation in vegetated conditions requires the coupling of backscatter models for bare soil and for vegetation (Zhang et al., 2021). One of the most popular models is the semi-empirical Water Cloud Model (WCM) (Attema and Ulaby, 1978), which requires external vegetation descriptors and a specific parameterization for the local conditions. This case is even more complex, although recent progress is being made in the transferability of model parameters to the regional scale (Benninga et al., 2022).

The launch of the Sentinel-1 satellites in 2014 and 2016 opened new possibilities for the estimation of SM at high spatial resolution. Their unprecedented compromise between high spatial resolution, frequent revisit time and radiometric accuracy (Torres et al., 2012), along with the open data distribution policy and the operational vocation of the Copernicus program, fostered the development of new methods for SM estimation, or the adaptation of existing ones, to the characteristics of Sentinel-1 data. In particular, the development of retrieval methods based on change detection techniques that evaluate backscatter changes between consecutive observations has made significant progress. The main hypothesis of these methods is that if time series are dense enough, the backscatter differences between consecutive observations might only be caused by SM variations, since the other variables affecting backscatter, e.g. soil roughness and vegetation, could be considered constant during such a short period. Following this idea, different approaches have been developed, such as the Short Term Change Detection (STCD) approach (Balenzano et al., 2021, 2011) or the TU Wien Change Detection (TUWCD) model (Bauer-Marschallinger et al., 2019; Wagner et al., 1999). On the other hand, some other methods following different principles have also been applied to Sentinel-1 data, such as Bayesian approaches (Notarnicola, 2014; Notarnicola et al., 2006) or machine learning algorithms like random forest regression (Liu et al., 2021), support vector regression (SVR) (Pasolli et al., 2011) or artificial neural network (ANN) (Baghdadi et al., 2012). Recently, a retrieval method that combined the sliding window approach (Balenzano et al., 2021) with physical scattering models in a stochastic ensemble inversion was proposed (Zhu et al., 2023) with very promising results.

At present, some of these approaches are applied to routinely produce SM products at scales of ~1 km (Balenzano et al., 2021; Bauer-Marschallinger et al., 2019), which significantly improve the spatial resolution of radiometer or scatterometer based products (Zappa et al., 2022). However, for some agricultural applications such as irrigation scheduling, this spatial resolution might still be too coarse, and SM values at the field scale are ideally sought (Gao et al., 2018; Le Page et al., 2020; Modanesi et al., 2022). Furthermore, field size varies significantly around the World (White and Roy, 2015) and many agricultural areas particularly in Africa, Asia and Europe are smallholders (< 2 ha) (Lesiv et al., 2019), where high resolution is a necessity for remote sensing to be useful to farmers.

Therefore, the applicability and the performance of different SM estimation approaches at the field scale still need to be evaluated. The objective of this work is to evaluate different SM estimation approaches based on Sentinel-1 data for wheat fields. Three change detection approaches were selected: the STCD approach (Balenzano et al., 2011), the TUWCD model (Wagner et al., 1999) and a multitemporal Bayesian change detection (MTBCD) algorithm (Notarnicola, 2014). These approaches were calibrated on eight experimental fields with available SM measurements, and some methodological adaptations were proposed to enhance their applicability to the particular case of wheat fields. Furthermore, the influence of vegetation on backscatter, and hence on SM retrievals, was accounted for by comparing the results obtained with the original Sentinel-1 time series and those obtained after applying the wheat attenuation correction method (WATCOR) recently proposed by Arias et al. (2022b).

2. Materials and methods

2.1. Study area and soil moisture measurements

The study focused on eight winter wheat test fields located in the province of Navarre (Spain) (Fig. 1). Navarre is a small but diverse province regarding climate, topography and land use. Therefore, it is divided in seven agricultural regions (Arias et al., 2020), where conditions for crop growth are expected to be rather constant. Two test fields were located in region R3 (rather wet, classified as Cf2b according to Köppen climate classification: average annual temperature (T_a) of 12.5ºC and annual rainfall (R_a) of 900 mm), four in region R5 (intermediate, with Csb climate class: $T_a = 12.7$ºC and $R_a = 655$ mm) and two in region R6 (dry, with Csa climate class: $T_a = 14$ºC and $R_a = 350$ mm). Two fields were monitored per agricultural year (2017–2018: fields 1 and 2; 2018–2019: fields 3 and 4; 2019/2020: fields 5 and 6; 2020/2021: fields 7 and 8). Each year, field pairs were managed exactly the same in terms of soil preparation, sowing and agricultural management (fertilization and other agrichemicals), except for irrigation, with half of them (odd field numbers) rain-fed and the other half irrigated (even field numbers). The irrigation system used was sprinkler irrigation, with a sprinkler spacing of 15mx18m, a design pressure of 3 kg/cm^2 and an application rate of 6 mm/h that lead to an irrigation uniformity of ~90%. Irrigation shifts are scheduled at night. Table 1 provides additional details.

Several (3 − 6) capacitance SM probes (Sentek Sensor Technologies, Stepney SA 5069, Australia) were installed on each field in winter and they were removed just before harvest (Table 1). These probes recorded volumetric SM every 30 min at 6 different depths, from the soil surface down to 60 cm deep. The top-most measurements (10 cm) were used in this study, so a basic assumption of this study is that SM is invariant in the top 10 cm of the soil. This is important, because Sentinel-1 sensing depth might vary from 1 cm to 10 cm approximately depending on the actual SM content of the soil (Ulaby et al., 1996). For each field, the median SM time series of all the probes installed on it was calculated. Then, these time series that had a 30 min temporal resolution, were confronted with Sentinel-1 acquisition dates and times, selecting only the measurements closest to each Sentinel-1 acquisition. The final number of measurements used, depended on the availability of Sentinel-1A and Sentinel-1B on each of the three orbits that over-flew the study area, i.e. 103ASC, 8DESC and 81DESC, at best ~30 acquisitions were available per orbit (Table 2).

Surface SM dynamics varied quite strongly in the different test fields (study years) (Fig. 2). Rain-fed fields normally experienced a transition from wet conditions in winter to dry soils in May-June (e.g., fields 1 and 7) (Fig. 2a and g). However, this was not always the case, and field 3 (Fig. 2c) had already quite dry conditions in winter. Field 5 (Fig. 2e) in turn, recorded frequent and significant precipitations during the spring,

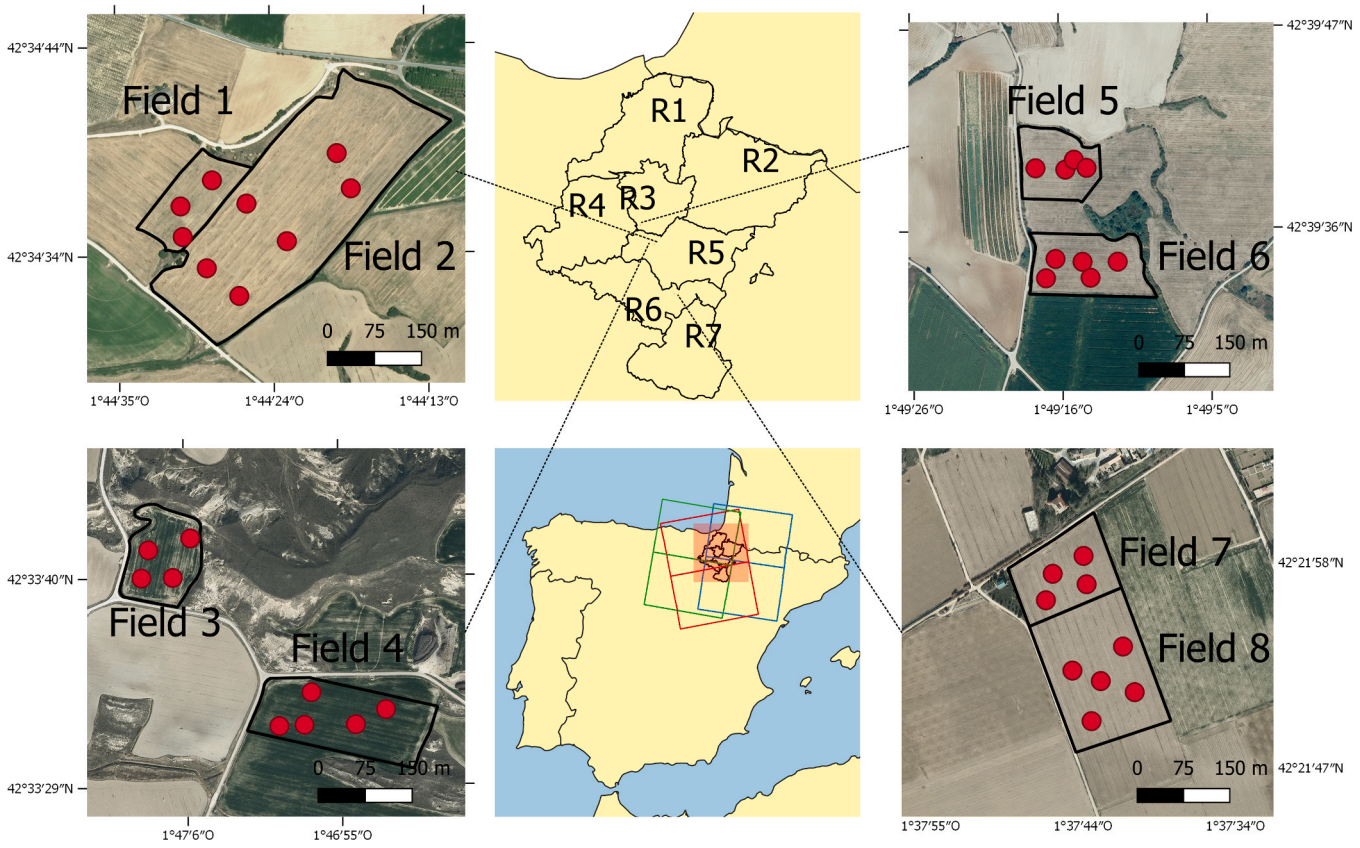

Fig. 1. Location of the test fields and agricultural regions of Navarre. Red points represent the location of soil moisture probes. Red, green and blue frames represent the footprints of 103ASC, 81DESC and 8DESC Sentinel-1 orbits, respectively. R1-R7 refer to the seven agricultural regions.

Table 1
Characteristics of the test fields. Rainfall and irrigation data comprises the period from sowing to harvest.

ID	Area (ha)	Texture class	% Sand	%Clay	Type	Rainfall + irrigation (mm)	Sowing	Harvest	Number of probes
1	1.4	Clay-loam	21.2	39.5	Rain-fed	537	25/10/2017	05/07/2018	3
2	8.5	Loam	31.2	26.7	Irrigated	637	25/10/2017	05/07/2018	6
3	1.6	Clay-loam	23.4	31.7	Rain-fed	331	25/10/2018	06/07/2019	4
4	2.8	Silt-loam	20.6	26.7	Irrigated	515	25/10/2018	06/07/2019	5
5	1.4	Clay	27.9	53.3	Rain-fed	352	11/12/2019	03/07/2020	4
6	1.9	Loam	30.8	26.9	Irrigated	438	11/12/2019	03/07/2020	5
7	1.8	Silty clay loam	10.8	28.2	Rain-fed	307	04/11/2020	15/07/2021	4
8	3.6	Silty clay loam	9.3	34.3	Irrigated	607	04/11/2020	15/07/2021	5

Table 2
Number of Sentinel-1 acquisitions available per field (ID) for each of the three orbits available; and start and end dates of the SM measurement periods.

ID	8DESC	81DESC	103ASC	Start date	End date
1–2	20	21	13	03/03/2018	27/06/2018
3–4	19	20	9	14/02/2019	21/06/2019
5–6	29	29	29	31/12/2019	28/06/2020
7–8	30	31	32	27/12/2020	02/07/2021

so no clear drying was observed. In general, irrigation management in fields 2, 4, 6 and 8 (Fig. 2b, d, f and h) avoided soil drying, however, keeping in mind that measurements were taken at the soil surface, quite rapid dynamics were observed, with SM increasing rapidly due to irrigation events and decreasing also quite rapidly afterwards.

2.2. Satellite imagery and data extraction

Fig. 3 summarizes all the satellite imagery and data needed for implementing the SM estimation techniques investigated, detailing the general and specific characteristics of each methodology. In the following sections, further details and explanations are given.

2.2.1. Sentinel-1 data

Sentinel-1 C-band SAR data was the base of this study, in particular the Interferometric Wide (IW) swath mode data, with a 250 km swath, 5 × 20 m spatial resolution and dual-pol (VH-VV) configuration, which is the pre-defined observation scenario over land in Europe. All available scenes from 1/September/2015–31/August/2021 covering the province of Navarre were downloaded as level-1 Ground Range Detected (GRD) products. These images corresponded to one ascending (103ASC) and two descending orbits (8DESC and 81DESC).

Images were processed with an automated pipeline implemented in SNAP Graph Processing Toolbox, which followed these steps: 1) thermal noise removal; 2) slice assembly; 3) apply orbit file; 4) calibration; 5) speckle filtering (3 ×3 Gamma-Map); 6) terrain flattening; 7) range-doppler terrain correction and 8) subset to the extent of Navarre. The terrain flattening and terrain correction step employed the SRTM 1 s

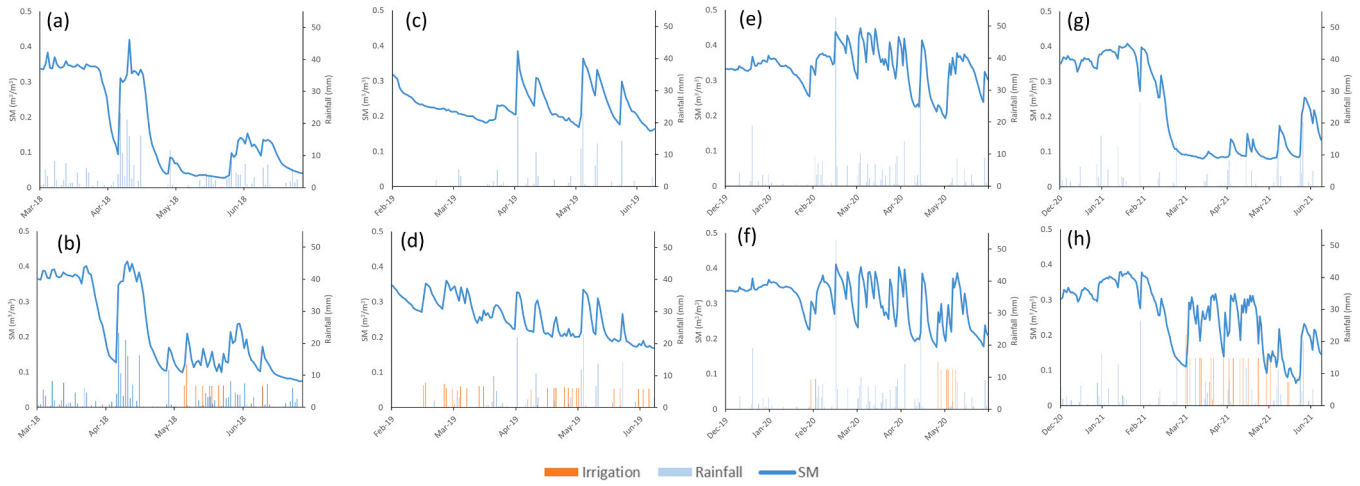

Fig. 2. Daily median volumetric SM at 10 cm depth (lines) and daily rainfall and irrigation (bars) for the eight test fields: (a) Field 1, (b) Field 2, (c) Field 3, (d) Field 4, (e) Field 5, (f) Field 6, (g) Field 7, (h) Field 8. Fields in the top row were rain-fed and those in the bottom row irrigated.

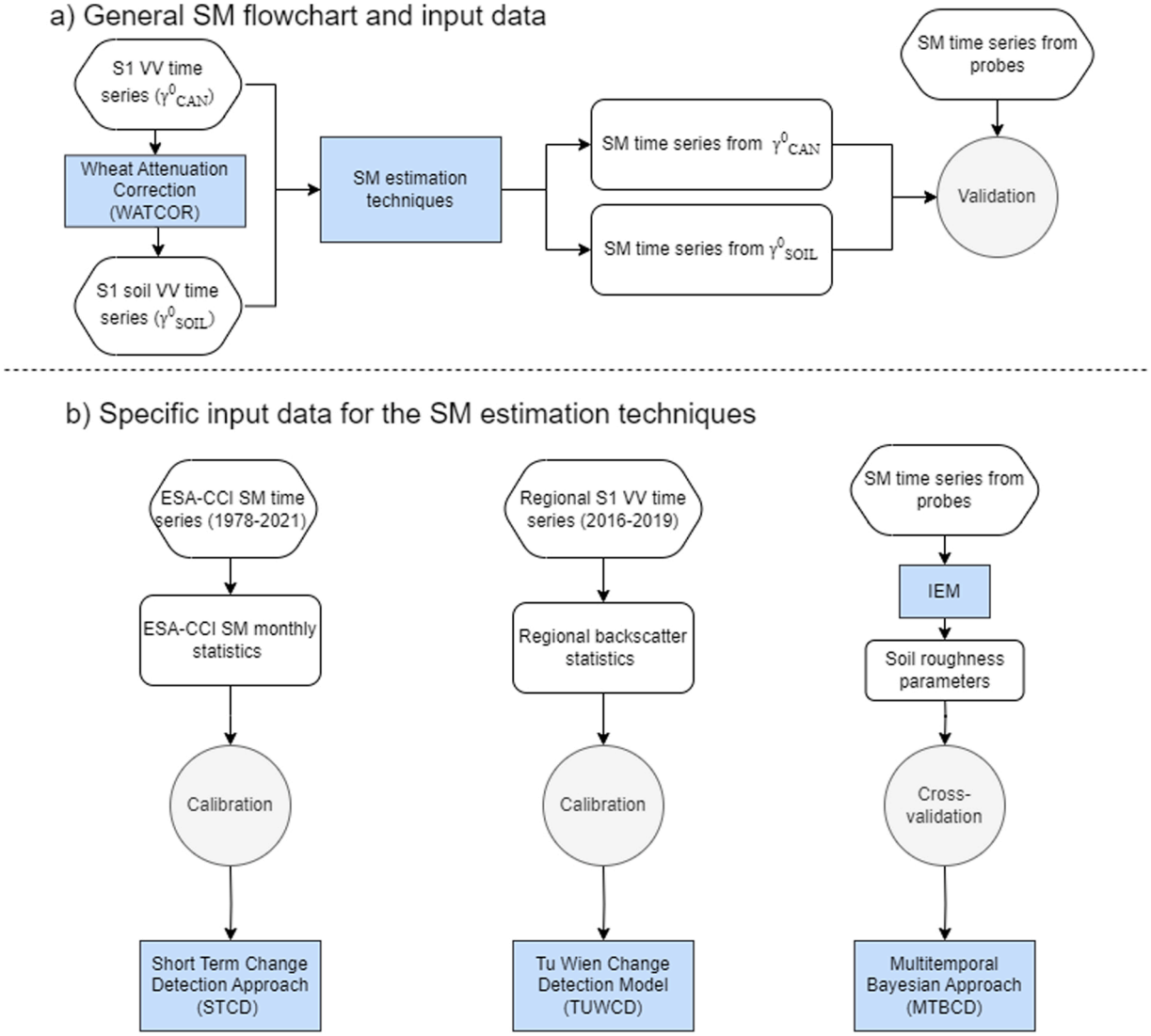

Fig. 3. a) General SM flowchart and input data and b) specific input data for the SM estimation techniques. CAN refers to canopy and WATCOR to the Wheat Attenuation CORrection method (Arias et al., 2022b).

HGT DEM. As a result, γ^0 backscatter coefficient images in VH and VV polarizations were produced, with a pixel size of 20 m. The projected local incidence angle was also obtained, as a secondary output for each scene.

For the eight test fields median backscatter coefficient values were extracted for each Sentinel-1 acquisition, resulting in backscatter time series in VV and VH polarizations. Prior to this, a 10 m inner buffer was applied to field boundaries to avoid mixed pixels. Two further processes were applied to the backscatter time series, firstly, the local incidence angle was normalized to a reference angle of $\theta = 40^0$ by applying an adapted version (Arias et al., 2022a) of the methodology proposed by (Mladenova et al., 2013). Secondly, the influence of wheat canopy in VV backscatter was corrected for with the WATCOR method (Arias et al., 2022b), obtaining a new VV backscatter time series corresponding to the soil, named γ^0_{SOIL}, which is assumed to be free of the influence of wheat vegetation cover, as opposed to the original backscatter time series γ^0_{CAN}, which corresponds to the complete wheat canopy. WATCOR removes the attenuation pattern produced by the wheat canopy in VV backscatter, based on the information contained in the backscatter time series itself, with no need for external information or parametrization (Arias et al., 2022b). Arias et al. (2022b) evaluated the performance of this method and found that it successfully eliminated wheat attenuation from Sentinel-1 backscatter time series, improving the correlation with ground measured SM and outperforming the results obtained by approaches based on the Water Cloud model.

2.2.2. ESA-CCI soil moisture product

The European Space Agency (ESA) provides a coarse resolution SM product through its Climate Change Initiative (CCI) (Dorigo et al., 2017). This ESA-CCI SM product is a global product containing daily SM estimates from 1978 until 2021 at a spatial resolution of 0.25°, based on active (scatterometers) and passive (radiometers) microwave sensors. Previous studies reported that the ESA-CCI SM product performed accurately (Wang et al., 2021; Zeng et al., 2015). In this study, the v06.1 level 3 combined SM product was used as ancillary data for the STCD approach. With this aim, the ESA-CCI SM time series of the pixels covering the test fields were downloaded and processed to obtain monthly statistics. In particular, the minimum, maximum and percentiles P05, P15, P25, P75, P85 and P95 were used.

2.2.3. Regional characterization of wheat backscatter

For calibrating the TUWCD model (see Section 2.3.2), a regional characterization of wheat backscatter was carried out. With this aim, a GIS database containing the field boundaries of all the EU Common Agricultural Policy (CAP) declarations in Navarre for years 2016, 2017, 2018 and 2019 was used, which was provided by the Department of Agriculture of the Government of Navarre. Wheat fields were extracted from this database and processed as follows: 1) create subsets for agricultural regions R3, R5 and R6; 2) mask out fields smaller than 0.5 ha; 3) apply a 5 m inner buffer to the field boundaries; 4) compute the median VV backscatter time series per field; 5) remove outliers (i.e., the 10% of fields most dissimilar to the median time series of all the fields on a region) (Arias et al., 2020); 6) normalize backscatter to a local incidence angle of $\theta = 40^0$ and apply WATCOR. After this process, backscatter time series of 13,200 wheat fields were obtained for region R3, 18,994 for region R5 and 11,401 for region R6; with this data a regional characterization of wheat backscatter was obtained by computing different percentiles of backscatter time series for each region (R3, R5 and R6) and orbit pass (103ASC, 8DESC and 81DESC).

2.3. Soil moisture estimation techniques

2.3.1. Short term change detection (STCD)

The STCD approach (Balenzano et al., 2011), is a change detection approach that uses dense time series (6–12 days revisit) of T co-polarized backscatter observations (γ^0_1, γ^0_2,…, γ^0_T) to estimate a SM time series (SM_1, SM_2,…,SM_T). The hypothesis of the methodology is that SM changes occur at a shorter temporal scale (days) than other parameters affecting the backscatter response (e.g. soil roughness, vegetation biomass or canopy structure), which vary at a longer temporal scale (weeks). Therefore, the ratio between two subsequent SAR observations (γ^0_2/γ^0_1) in linear units can be expressed as a function of the dielectric constant ε and the local incidence angle θ of each observation date (Eq. 1).

$$\frac{\gamma^0_2}{\gamma^0_1} \approx \left|\frac{\alpha_{pp,2}(\varepsilon,\theta)}{\alpha_{pp,1}(\varepsilon,\theta)}\right|^2 \tag{1}$$

where, α_{pp} is the Fresnel reflection coefficient at HH or VV polarization, and α_{VV} is defined as follows (Eq. 2).

$$|\alpha_{VV}(\varepsilon,\theta)| = \left|\frac{(\varepsilon-1)(\sin^2\theta - \varepsilon(1+\sin^2\theta))}{(\varepsilon \cos\theta + \sqrt{\varepsilon - \sin^2\theta})^2}\right| \tag{2}$$

For N observations there are N − 1 equations with N unknown Fresnel coefficients. A bounded least-squares optimization was used to solve the equation system (Balenzano et al., 2013). Once that the α time series were determined for the observations, the corresponding ε values were obtained and converted into volumetric SM values using the empirical expression of (Hallikainen et al., 1985).

The values of the boundary conditions (α_{min}, α_{max}) were found to play an important role in the retrieval accuracy (He et al., 2017). Ideally, (α_{min}, α_{max}) should correspond to the dynamic range of SM for the study area during the period of observation (Ouellette et al., 2017). In the literature different methods for constraining (α_{min}, α_{max}) can be found. For instance, some studies used fixed SM values (Balenzano et al., 2011), while others relied on SM field measurements (Zhang et al., 2018). Other authors used coarser scale SM values obtained from scatterometers or radiometers (Al-Khaldi et al., 2019; Ouellette et al., 2017; Zhu et al., 2022). In this study, the latter approach was followed, and thus (α_{min}, α_{max}) were derived from the ESA CCI SM product. With this aim, the monthly minimum and maximum ESA CCI SM values were initially considered (Supplementary materials 1), but they showed a rather low dynamic range (due to their coarser spatial scale), so additional schemes were tested enhancing the ESA CCI SM dynamic range. For this, the mean monthly SM variation range was estimated through a variable named SM_{diff} (Eq. 3). This variable was added or subtracted to the different ESA CCI SM monthly percentiles (Table 3) to find the combination optimally describing (α_{min}, α_{max}) boundary conditions.

$$SM_{diff} = \frac{\overline{(SM_{max.month} - SM_{min,month})}}{2} \tag{3}$$

Regarding the length of the time series considered, Palmisano et al. (2018) suggested sub-dividing the complete backscatter time series T in smaller blocks to avoid error propagation into SM estimations. Therefore, a sliding window of N backscatter observations was considered, and the average value of the estimations was calculated (Shi et al., 2021). Different values of N (4, 5, 6, 8, 12 and 18) were evaluated and the optimum was selected.

Therefore, the implementation of this approach had first a calibration phase that consisted in evaluating which combination of

Table 3
Schemes considered for the calibration of (α_{min}, α_{max}) boundary conditions based on ESA CCI SM statistics. P is the monthly SM percentile.

Scheme	Min SM value	Max SM value
A	Min	Max
B	P25 - SM_{diff}	P75 + SM_{diff}
C	P15 - SM_{diff}	P85 + SM_{diff}
D	P05 - SM_{diff}	P95 + SM_{diff}

(α_{min}, α_{max}) boundary conditions (Table 3) and N value provided the best results. After this calibration phase, scheme D and N = 4 were identified as optimal, so this was the option used in the study (Supplementary materials 2.1).

2.3.2. TU Wien change detection model (TUWCD)

The TUWCD model (Wagner et al., 1999) interprets backscatter changes in a time series as changes in soil moisture, while other surface properties (geometry, roughness, vegetation, etc.) are considered as static. This model is used to produce a global SM product at a resolution of 1 km (Bauer-Marschallinger et al., 2019). Here the algorithm is applied at the field scale, using Sentinel-1 backscatter time series of each field (see Section 2.2.1). This model defines the surface soil moisture content (SSM) as a relative index between 0 and 1, which is estimated from the backscatter value of that particular day normalized with some minimum and maximum backscatter boundary conditions (Eq. 4).

$$SSM(t) = \frac{\gamma^0(t) - \gamma^0_{min}}{\gamma^0_{max} - \gamma^0_{min}} \quad (4)$$

where, $\gamma^0(t)$ is the backscatter observation in dB units at time t, and γ^0_{min} and γ^0_{max} are the minimum and maximum backscatter values in dB units corresponding to dry and saturated soil conditions, respectively. These values are ideally extracted from long time series, where it is likely that the pixel or polygon of interest would reach these dry and saturated conditions some time (Wagner et al., 1999).

Bauer-Marschallinger et al. (2019) already mentioned that the relatively short length of the Sentinel-1 data record might result in an absence of the dry and saturated conditions required to successfully apply this algorithm. This might be particularly difficult in humid regions (Zribi et al., 2014) or in agricultural areas with irrigation systems, where completely dry conditions might never be met. Furthermore, in agricultural areas, more and more often managed under crop rotation schemes (European Commission, 2022), yearly varying crops might also influence backscatter dynamics (Arias et al., 2020; Veloso et al., 2017) making the selection of γ^0_{min} and γ^0_{max} very challenging. To overcome this problem, this study proposes a regional characterization of backscatter for wheat fields (Section 2.2.3). For each agricultural region, backscatter time series of thousands of wheat fields were obtained for four different years and their statistics (minimum, maximum and different percentiles) were computed and used to calibrate the algorithm, that is, to select the dry and wet references, evaluating different schemes (Table 4).

These different schemes were applied on a calibration phase to select the optimum (γ^0_{min}, γ^0_{max}). The results of this calibration (see Supplementary materials 2.2.) showed that scheme 3 was optimal. Backscatter values below or above the limits were set to 0 and 1 respectively (Hornáček et al., 2012). Then, relative SSM values were linearly scaled to SM values (m^3/m^3) (Carranza et al., 2019) (Eq. 5).

$$SM(t) = (SM_{sat} - SM_{wp}) * SSM(t) + SM_{wp} \quad (5)$$

where, SM_{sat} is the saturated soil moisture content, extracted from soil texture data (Rawls et al., 1982) and SM_{wp} is the wilting point, also estimated from soil texture data (Saxton and Rawls, 2006). The soil texture of the test fields (Table 1) was obtained by field sampling and laboratory analyses.

Table 4
Schemes for obtaining the dry and wet soil conditions (γ^0_{min}, γ^0_{max}) in the TUWCD model from the regional statistics of wheat fields time series. P is the backscatter percentile.

Scheme	γ^0_{min}	γ^0_{max}	Scheme	γ^0_{min}	γ^0_{max}
1	min	max	9	P0.01	max
2	min	P0.999	10	P0.01	P0.999
3	min	P0.99	11	P0.01	P0.99
4	min	P0.9	12	P0.01	P0.9
5	P0.001	max	13	P0.1	max
6	P0.001	P0.999	14	P0.1	P0.999
7	P0.001	P0.99	15	P0.1	P0.99
8	P0.001	P0.9	16	P0.1	P0.9

2.3.3. Multitemporal Bayesian change detection approach (MTBCD)

The MTBCD is an inversion procedure for SM estimation based on the Bayes' theorem, adapted from (Notarnicola, 2014). The objective is to infer the unknown soil dielectric constant time series ($\varepsilon_1, \varepsilon_1, \ldots, \varepsilon_T$) from the available Sentinel-1 backscatter time series ($\gamma^0_1, \gamma^0_2, \ldots, \gamma^0_T$). By applying Bayes' theorem, it is possible to turn probabilities estimated from a training dataset into probabilities for the estimation of the unknown variable ε (Gelman et al., 2013).

The conditional probability density function (pdf) $P(\gamma^0_1, \gamma^0_2, \ldots, |\varepsilon_i)$, which is the probability of finding the vector of γ^0_i given specific values of ε_i, is estimated from a training set of backscatter values and their corresponding values of ε. By using the Integral Equation Model (IEM) (Fung, 1994), the theoretical backscatter values $\gamma^0_{i,IEM}$ calculated from the ground SM measurements were obtained. These values were compared to the Sentinel-1 backscatter values introducing a random variable R that accounts for the sensor noise and model errors (Notarnicola et al., 2008) (Eq. 6).

$$\gamma^0_i = R\gamma^0_{i,IEM} \quad (6)$$

The pdf of R is assumed to follow a Gaussian distribution (Eq. 7), and its mean (μ) and standard deviation (σ), are determined by using the maximum likelihood principle. Tests were carried out to check whether this distribution adequately represents the data (Notarnicola et al., 2008).

$$P(R) = \frac{e^{-(R-\mu)^2/2\sigma^2}}{\sqrt{2\pi}\sigma} \quad (7)$$

Once that the pdf parameters were calculated, the Bayes' theorem from two consecutive γ^0_1, γ^0_2 observations for obtaining the conditional density function $P(\varepsilon|\gamma^0_1, \gamma^0_2)$ was applied (Eq. 8).

$$P(\varepsilon|\gamma^0_1, \gamma^0_2) = \frac{P_{prior}(\varepsilon) P_{post}(\gamma^0_1, \gamma^0_2|\varepsilon)}{P(\gamma^0_1, \gamma^0_2)} \quad (8)$$

where, P_{prior} is the a priori joint density function for ε, which can be assumed to follow a uniform density function over the physical range of the parameter. $P_{post}(\gamma^0_1, \gamma^0_2|\varepsilon)$ is the posterior density function based on measured values. $P(\gamma^0_1, \gamma^0_2)$ is a normalization factor.

$P(\varepsilon|\gamma^0_1, \gamma^0_2)$ can be expressed in terms of the probability density $P(R)$ by a transformation detailed in (Notarnicola et al., 2006). The optimal estimator $\bar{\varepsilon}$ for ε, which has de minimum variance is the conditional mean (Eq. 9).

$$\bar{\varepsilon} = \frac{\int (\varepsilon - \varepsilon_{min}) P_{prior}(\varepsilon) \left(\frac{1}{\gamma^0_{IEM}}\right)^2 P\left(\frac{\gamma^0_1}{\gamma^0_{IEM}}\right) P\left(\frac{\gamma^0_2}{\gamma^0_{IEM}}\right) d\varepsilon}{P(\gamma^0_1, \gamma^0_2)} \quad (9)$$

where, ε_{min} is the minimum value of the uniform density function from P_{prior}.

This approach needs to be trained and validated. For this IEM simulations were used. Since the IEM requires as input not only ε but also soil roughness parameters s (standard deviation of heights) and l (correlation length), and soil roughness measurements were not available for this study, s and l were optimized. In total, 414 combinations of soil roughness parameters were evaluated: s (from 0.2 cm to 2 cm with a step of 0.1 cm) and l (from 2 cm to 25 cm with a step of 1 cm). For each combination of s and l, the backscatter values were simulated using as input the available SM measurements. Then, the optimization function selected the combination of roughness parameters that minimized the RMSE between the observed and simulated backscatter values, being

$s = 0.4$ cm and $l = 3$ cm (see Supplementary Materials 2.3).

The training phase consisted in determining the pdf parameters that were later used for SM estimation. In this case, a 4-fold cross-validation scheme was performed separately for each orbit pass, with 6 fields used for training and 2 for validation in each fold.

2.4. Evaluation of results

The performance of the evaluated SM retrieval techniques was assessed with different metrics (Entekhabi et al., 2010b) calculated between the volumetric SM recorded by the probes (SM_{obs}) and the estimated SM (SM_{est}) with each technique: Pearson correlation (R), root-mean-square error (RMSE), bias and unbiased root-mean-square error (ubRMSE). The typical target accuracy threshold defined for low resolution missions (e.g, SMOS or SMAP) is ubRMSE ≤ 0.04 m^3/m^3 (Gruber et al., 2020).

Each SM_{est} value was compared with the SM_{obs} ground measurement closest to its acquisition time. In the evaluation of results, performance metrics were reported for each change detection technique and for each test field. Furthermore, the eventual influence that some scene acquisition and field conditions might have in the results were evaluated, in particular: the Sentinel-1 orbit considered, the rainfed or irrigated status of the field, the month of the year and the wetness of the field.

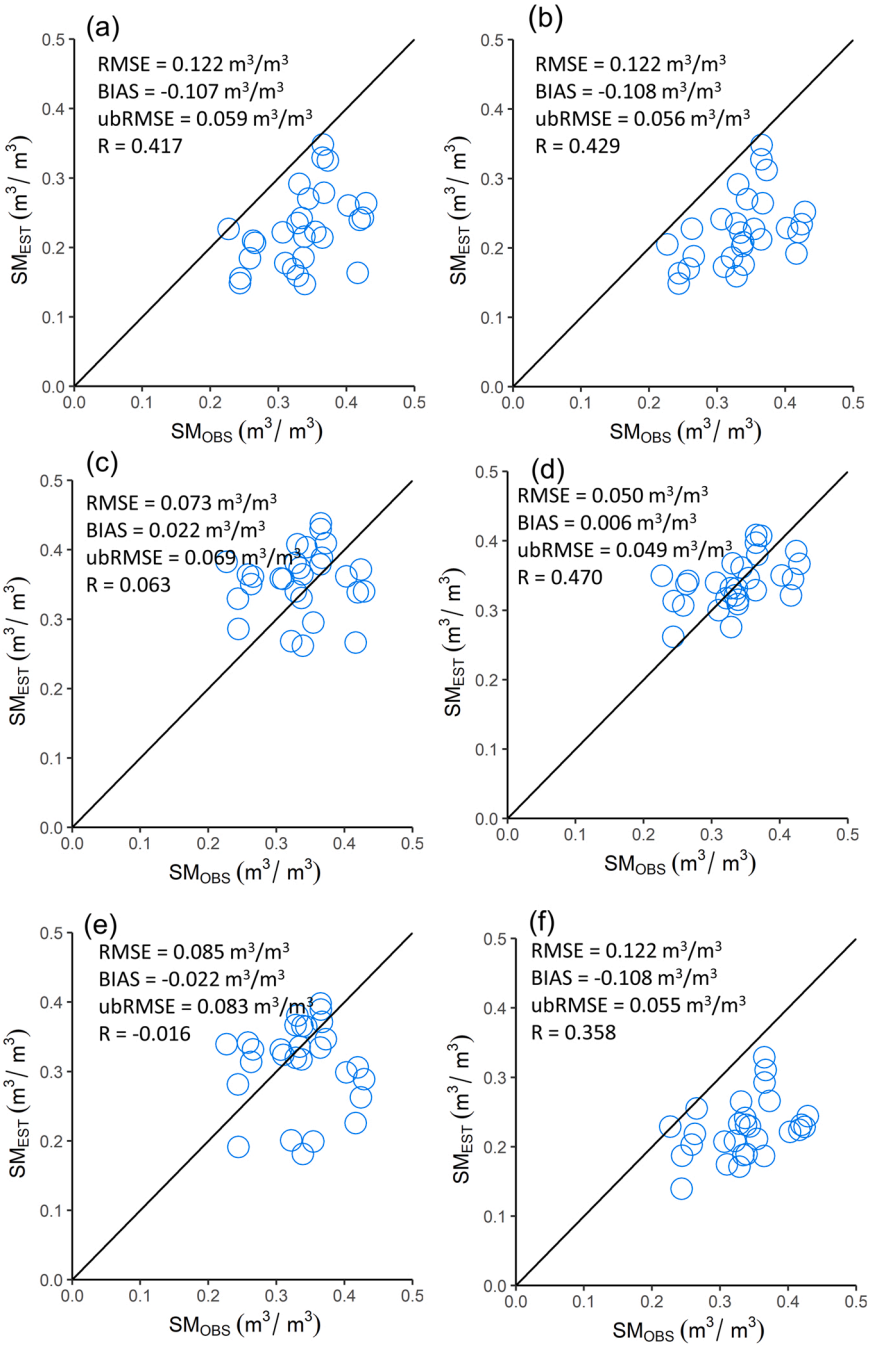

Fig. 4. Scatterplots of estimated SM versus observed SM for the different methodologies for a sample plot (field 5 and orbit pass 8DESC). (a) STCD (γ^0_{CAN}); (b) STCD (γ^0_{SOIL}); c) TUWCD (γ^0_{CAN}); (d) TUWCD (γ^0_{SOIL}); (e) MTBCD (γ^0_{CAN}); (f) MTBCD (γ^0_{SOIL}).

3. Results

3.1. Comparison between methodologies

In this section, the global statistical results obtained for each methodology are presented. The numerical results for every field and orbit pass, using as input both the γ^0_{CAN} and γ^0_{SOIL} time series, can be found in Supplementary Materials 3. As an example, the results of a sample field (field 5) are shown here (Fig. 4), where best results were obtained with TUWCD and γ^0_{SOIL}.

Fig. 5 shows the results of all the fields, after computing the performance metrics per orbit pass and field. Points not only represent the different test fields (colors), but also the Sentinel-1 orbit pass used in each case (symbols). Boxplots represent all the point data, summarizing the median and quartiles of the performance metrics obtained for each approach.

Median values of the performance metrics demonstrate a positive effect of the vegetation correction in all techniques. In particular, γ^0_{SOIL} metrics improved those obtained with γ^0_{CAN} in the TUWCD and MTBCD approaches and to a much lesser extent in the STCD. Different metrics provide different views on the performance of the techniques, regarding the RMSE best results were obtained with the TUWCD (0.08 m^3/m^3), followed by STCD (0.09 m^3/m^3) and MTBCD (0.12 m^3/m^3). STCD and MTBCD had negative bias and TUWCD a positive one. Looking at the unbiased ubRMSE, the TUWCD approach also provided the best results (0.06 m^3/m^3) but practically matched by the MTBCD, and then followed by STCD (0.08 m^3/m^3). In turn, the highest correlation values were obtained by the MTBCD approach (0.52), followed by TUWCD (0.46) and STCD (0.45).

Looking at field results in detail, it can be observed that results varied from case to case, with rather large variability ranges for all the metrics: RMSE (0.05 – 0.17 m^3/m^3), bias (−0.16 to 0.12 m^3/m^3), ubRMSE (0.04

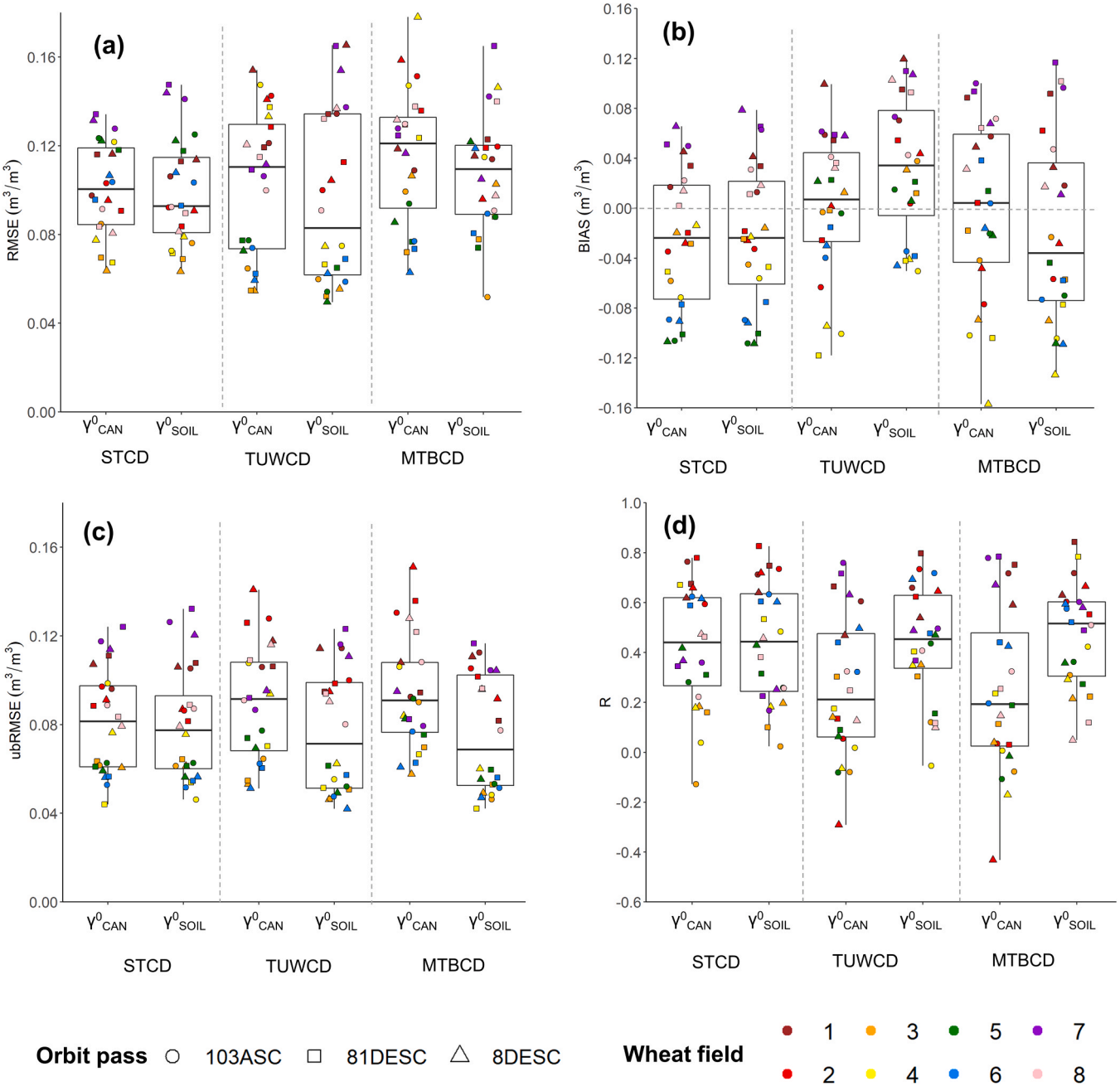

Fig. 5. Statistical results for the different SM estimation techniques. (a) RMSE; (b) bias; (c) ubRMSE; (d) Correlation.

– 0.15 m^3/m^3) and R (−0.4 to 0.9). The approaches with the highest variability were TUWCD and MTBCD. On the other hand, STCD provided more consistent results and had a lower variability. This field-to-field variability might be related to the particular characteristics of each field, for instance, fields 1, 7 and 8, all had a positive bias, indicating a systematic overestimation of SM. Conversely, fields 3, 4, 5 and 6 had a negative bias (except for TUWCD). The correlation values have to be interpreted with care, as they depend on the dynamic range of SM for each field. For instance, field 3 showed poor R values but successful results in terms of bias, RMSE and ubRMSE.

For a more in-depth analysis, the results obtained with each method run with γ^0_{SOIL}, were examined to evaluate the influence of different factors on the retrievals. The selected factors were the agricultural water management (rain-fed or irrigated), the satellite orbit passes, the month

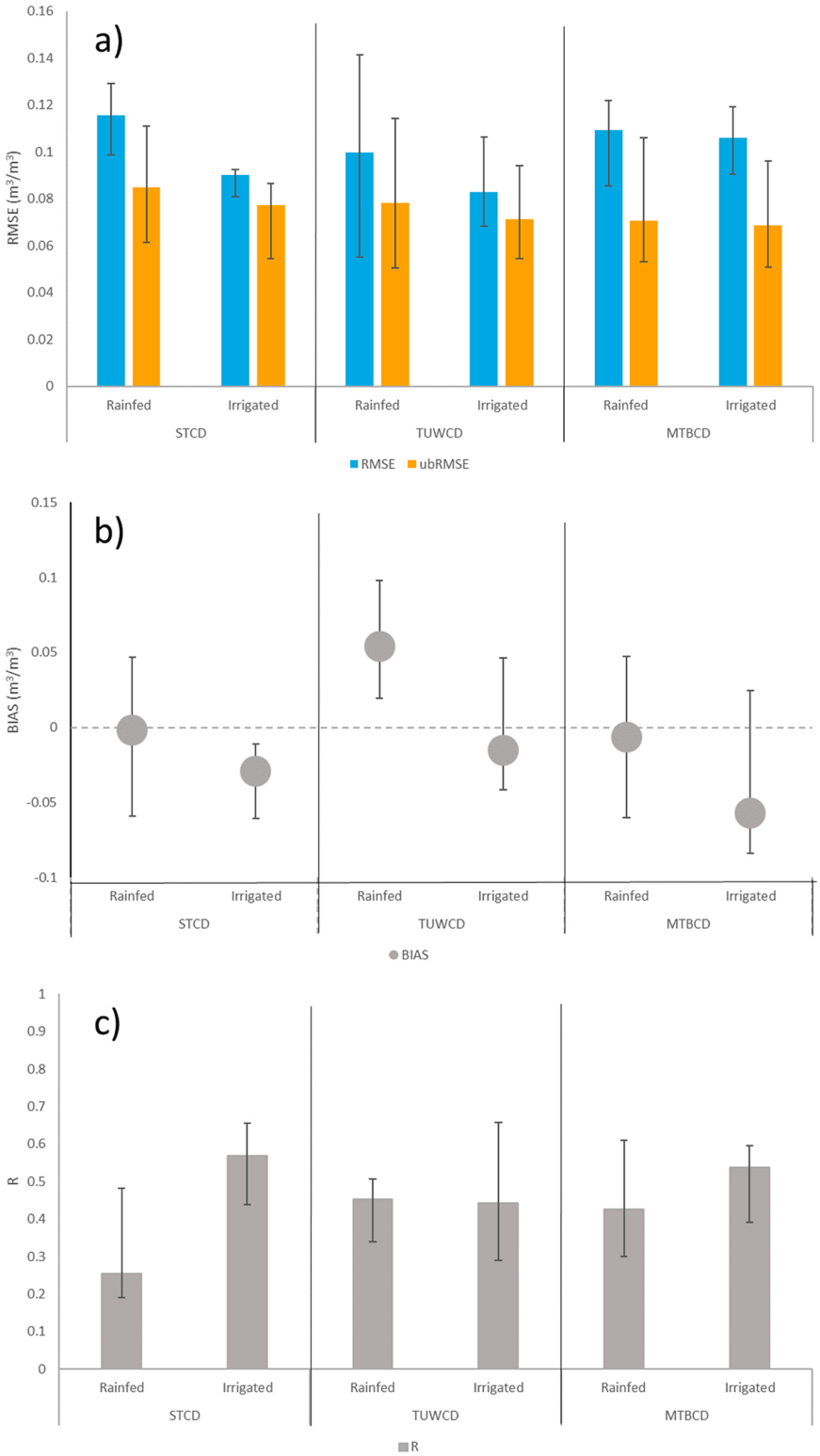

Fig. 6. Statistical results for the different SM estimation techniques depending on irrigation. (a) RMSE and ubRMSE; (b) Bias; (c) Correlation.

of the year and the soil moisture content.

3.2. Comparison between rain-fed and irrigated fields

The results based on the agricultural water management are shown in Fig. 6. RMSE metrics did not differ greatly between rain-fed and irrigated fields for MTBCD (~0.10 m^3/m^3). However, for STCD and TUWCD approaches, the RMSE was lower in irrigated fields. In general, RMSE variability (error bars in Fig. 6a) was larger for rain-fed fields. Regarding the ubRMSE, all techniques achieved similar median results (~0.08 m^3/m^3) with slightly lower errors for irrigated conditions. Specifically, fields 1, 2, 7 and 8 had higher ubRMSE (>0.08 m^3/m^3) than fields 3, 4, 5 and 6 (ubRMSE ~0.05 m^3/m^3) (see Supplementary materials 3). In terms of correlation, STCD and MTBCD showed higher

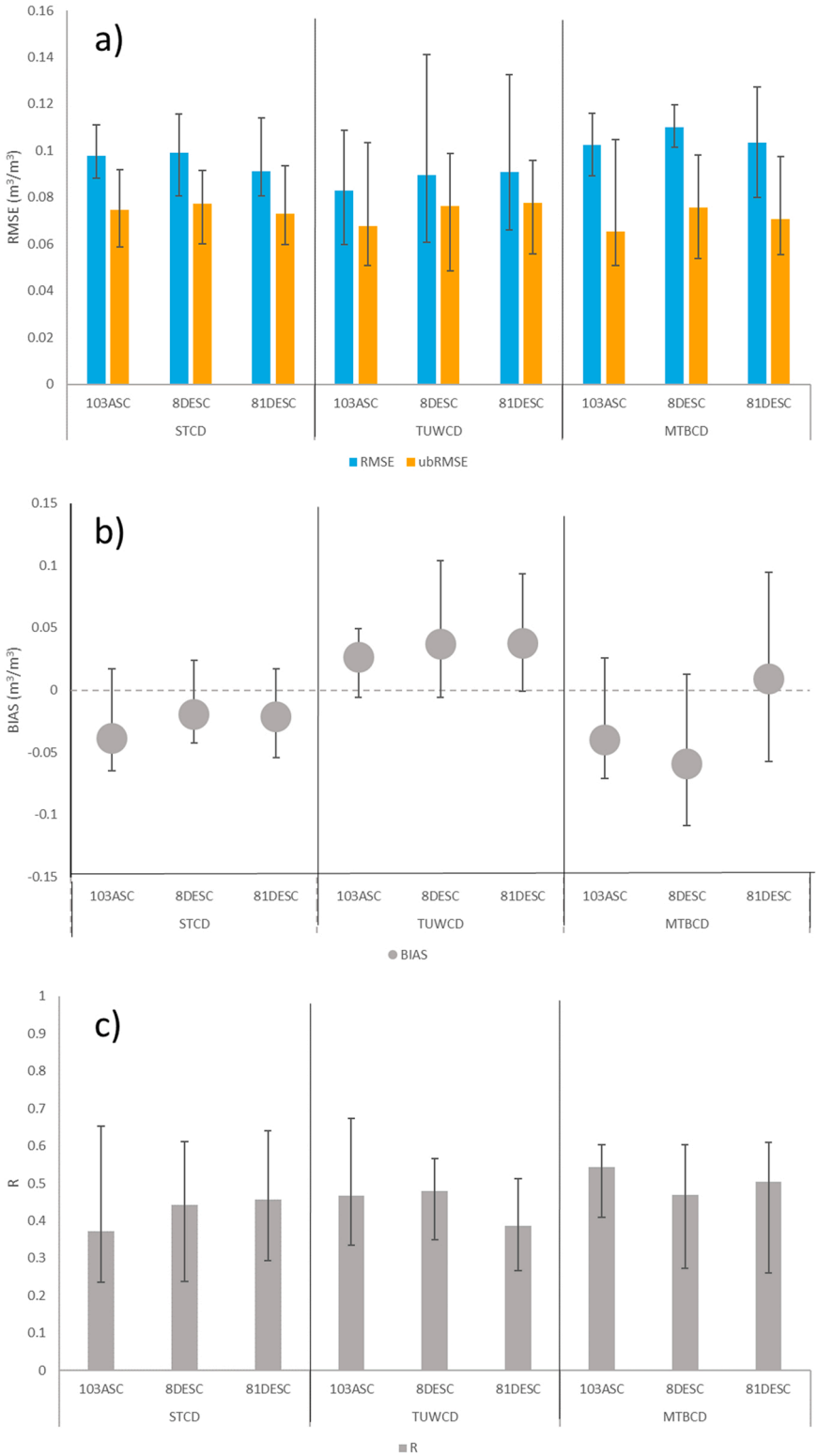

Fig. 7. Statistical results for the different SM estimation techniques depending on the orbit. (a) RMSE and ubRMSE; (b) Bias; (c) Correlation.

correlation values for irrigated fields, whereas TUWCD did not show any clear difference.

3.3. Comparison between orbit passes

The performance metrics obtained for the three orbit passes (Fig. 7) did not show clear differences. In general, for each SM estimation technique the values of the performance metrics obtained for the three orbit passes were similar. In terms of ubRMSE results were slightly better for the ascending pass in TUWCD and MTBCD, but differences were minor. For TUWCD descending orbits showed a larger variability in terms of RMSE and bias than the ascending one. Correlation results showed minor differences with slightly lower correlations for the ascending orbit in STCD but slightly higher in MTBCD. In any case these differences were not significant, and performance metrics seemed to vary more strongly depending on the particular field than on the orbit pass.

3.4. Evaluation of results per month

Median performance metrics were computed per month to assess the eventual influence of the scene acquisition month on the accuracy (Fig. 8). Correlation results in this case are omitted, since the SM dynamic range on each month was too small to provide reliable values.

There were clear differences depending on the month, particularly for TUWCD and MTBCD. RMSE values were lowest in winter months (January and February) for all cases, with values below 0.05 m^3/m^3 for TUWCD and MTBCD. In STCD, the RMSE was slightly higher (0.075 m^3/m^3). The RMSE in March was higher for all methods except for MTBCD, and April, May and June obtained the highest errors in all cases (0.08 – 0.12 m^3/m^3). RMSE was exceptionally high in June in the MTBCD (0.13 m^3/m^3). Regarding ubRMSE results, TUWCD presented very low values in January and February (< 0.02 m^3/m^3), while the remaining months had higher values that did not exceed 0.05 m^3/m^3. MTBCD also had a very good result in January (< 0.02 m^3/m^3), intermediate ones in February, March and April (~0.035 m^3/m^3), and higher errors in May and June (0.05 – 0.06 m^3/m^3). Finally, STCD was the approach that had overall the highest ubRMSE results, with a less marked difference between months, although winter months had also the lowest errors.

3.5. Evaluation of results depending on soil moisture content

With the aim of evaluating the performance of the retrieval methods depending on the actual soil moisture content of fields, the median performance metrics were computed for three SM levels: dry (<0.15 m^3/m^3), intermediate (0.15 m^3/m^3 – 0.30 m^3/m^3) and wet (> 0.30 m^3/m^3). The median RMSE results (Fig. 9) showed certainly high error values for dry conditions in all the techniques (0.013 – 0.18 m^3/m^3). Wet conditions also presented relatively high RMSE metrics, but not as high as in the dry case (0.09 – 0.011 m^3/m^3), except for the TUWCD that achieved the best results in wet conditions (RMSE = 0.06 m^3/m^3).

In general, the best results were achieved with intermediate moisture conditions, with RMSE ~0.06 m^3/m^3 for the STCD, TUWCD and MTBCD. All approaches presented a high positive bias (>0.12 m^3/m^3) for dry conditions, conversely bias was negative for wet conditions (−0.05 to −0.1 m^3/m^3). Intermediate conditions obtained the lowest bias for all approaches. Unbiased RMSE values (ubRMSE) were similar for the four techniques (0.03 – 0.05 m^3/m^3) and did not depend on the actual moisture conditions.

These results showed that, depending on the actual SM content, the approaches could overestimate or underestimate SM. In Fig. 10, SM time series for different test fields are displayed to show the behavior of the different approaches. Fig. 2 shows that fields 1 and 2 had a similar SM content during January and February, and then, SM dropped dramatically in field 1, whereas SM remained slightly higher in field 2 due to irrigation. In this case, although the evaluated approaches were sensitive to the precipitation event and subsequent soil wetting in April 2018,

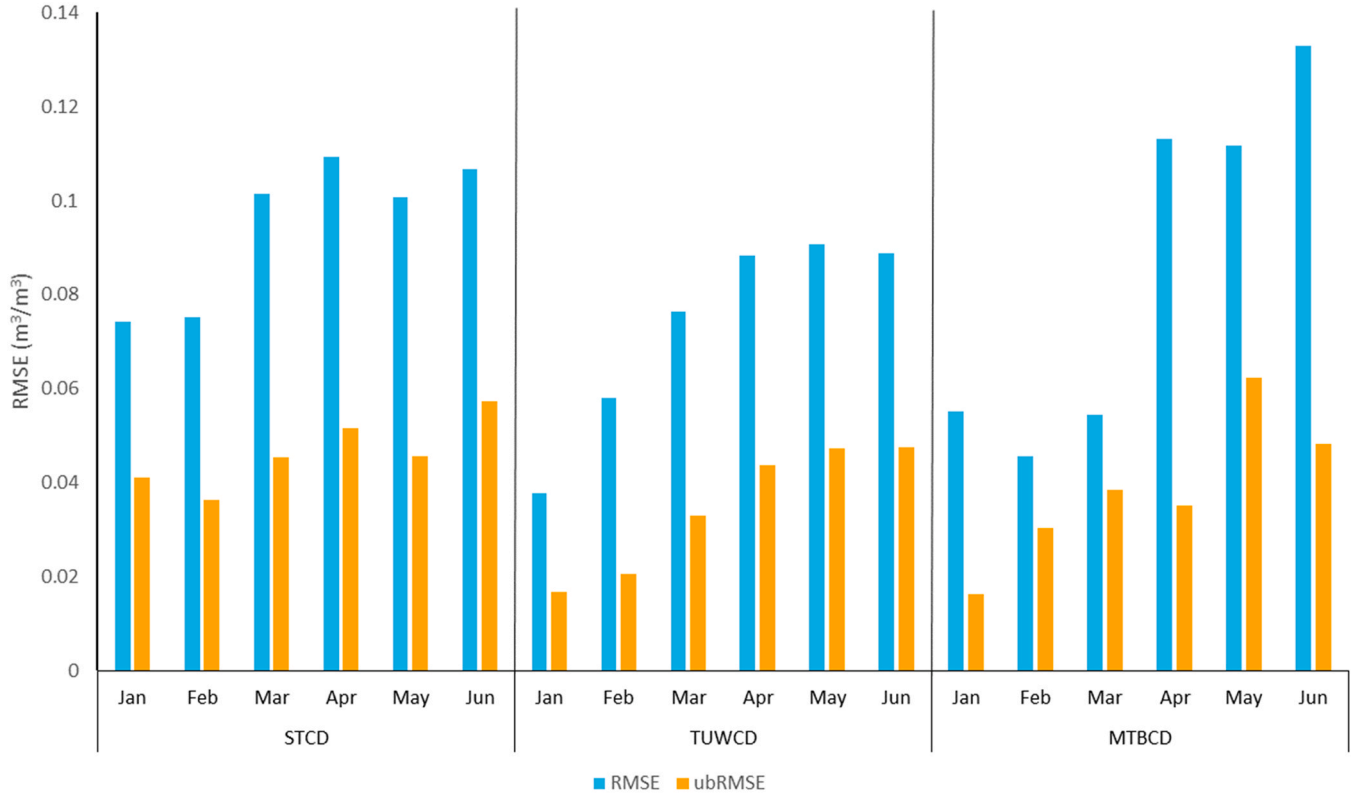

Fig. 8. Median RMSE and ubRMSE results for the different SM estimation techniques and months.

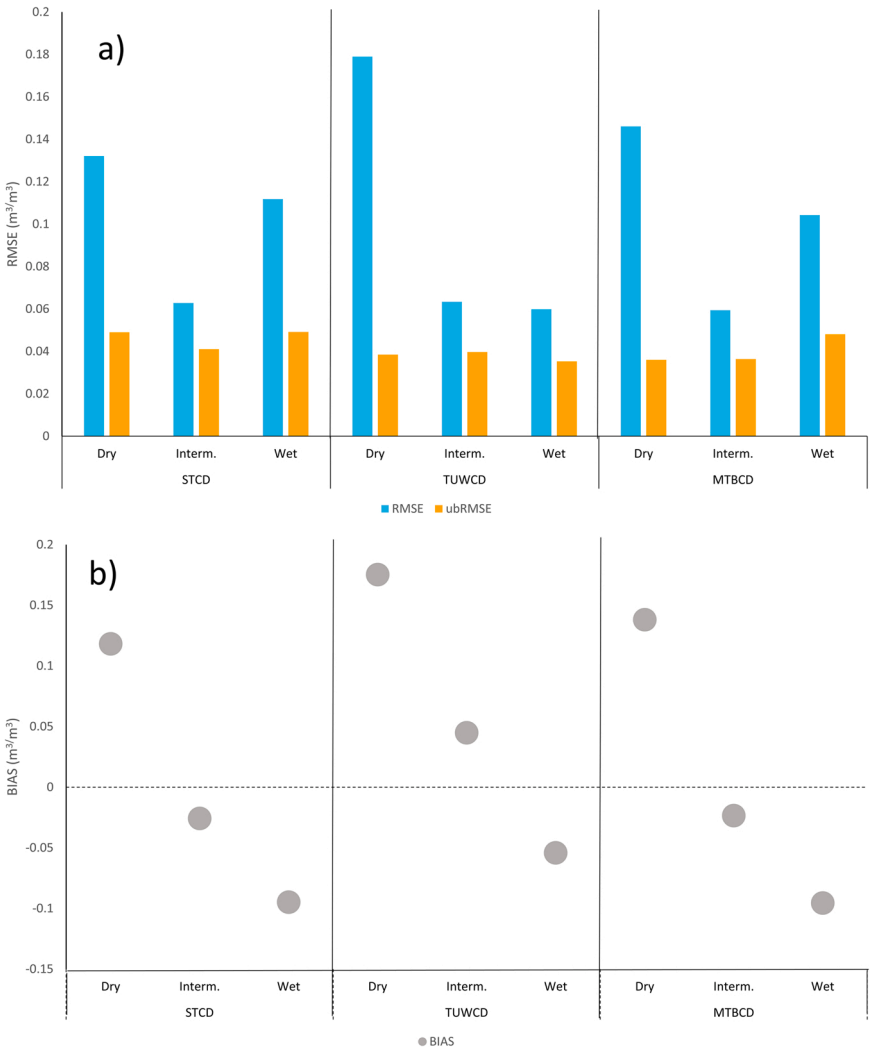

Fig. 9. a) RMSE, ubRMSE and b) Bias results for the different SM estimation techniques depending on the SM conditions. Bars represent median values.

they did not predict adequately the significant drying of field 1 (Fig. 10a). MTBC and STCD approaches estimated SM better in the irrigated Field 2 (Fig. 10b). On the other hand, fields 3, 4, 5 and 6 had rather high SM (Fig. 2), and although field 6 was under irrigation, it showed slightly lower SM values than field 5 because precipitations were abundant that season. For these fields, TUWCD provided the best estimations, predicting a range of SM values similar to measurements and showing sensitivity to some wetting and drying events throughout the season (Fig. 10c-f). STCD and MTBC also showed some sensitivity to SM dynamics, but their SM estimates were severely biased (underestimated). Similarly to field 1, field 7 also had an extreme SM drop in March, and neither of the approaches was able to estimate these low SM conditions from March to May (Fig. 10g). Although field 8 also presented a SM drop as field 7 did, the estimations were better because SM was higher during spring months due to irrigation events. In this field, TUWCD had the highest bias because it predicted a high SM level almost the whole period (Fig. 10h).

4. Discussion

The comparative analysis between the three methodologies demonstrated clear benefits after vegetation correction for TUWCD and MTBCD. In STCD the results were similar with and without vegetation correction, so this pre-processing step might be omitted. Earlier studies already demonstrated that vegetation dynamics and, eventually, surfaces roughness changes might have a substantial effect on TUWCD results (Zhu et al., 2019). On the other hand, STCD obtained optimal results when a sliding window of N = 4 was considered. As N increased, results worsened, this can be interpreted as a smoothing effect of N on SM estimates, blurring the short-term SM dynamics. Other researchers stated that large N values might foster error propagation in the algorithm (Palmisano et al., 2018), and provide SM estimates affected by changing surface and vegetation conditions in the mid-term (Balenzano et al., 2011).

The overall performance metrics showed that there was not any approach that clearly outperformed the rest. The four approaches obtained median RMSE values ranging from 0.08 to 0.11 m^3/m^3. In terms of bias, the TUWCD appeared to have a different behavior, as positive bias was found in most test fields, contrary to the rest of techniques were negative bias predominated. Median Pearson correlation values ranged from 0.44 to 0.55, but the interpretation of these results had to be done with care, since the actual soil moisture dynamic range of each field during the agricultural season might influence correlation. In terms of ubRMSE results were also very similar with TUWCD and MTBCD achieving a median value of 0.07 m^3/m^3, and STCD of 0.08 m^3/m^3. The statistical results of this study are comparable to other works. Attarzadeh et al. (2018) obtained RMSE values ~0.06 m^3/m^3 when fitting a SVR at the field scale using as input both Sentinel-1 and Sentinel-2 features. Benninga et al. (2020) used a calibrated version of the IEM to obtain field scale SM estimations in sparsely vegetated soils with

Fig. 10. Ground SM time series and estimated SM using the different approaches with orbit 8DESC: a) Field 1; b) Field 2; c) Field 3; d) Field 4; e) Field 5; f) Field 6; g) Field 7 and h) Field 8.

RMSE values of 0.08 – 0.11 m^3/m^3. Also, working at the field scale, Amazirh et al. (2018) obtained a RMSE of 0.16 m^3/m^3 with TUWCD. Even at coarser resolutions, medium correlation values and intrinsic RMSE of ~0.07 m^3/m^3 was obtained after applying STCD in larger areas (Balenzano et al., 2021) and RMSE in the range 0.08–0.12 m^3/m^3 was obtained in vegetated areas (Pulvirenti et al., 2018). Using other SM estimation methods, similar results were also found in wheat (Ma et al., 2020) or in cropland areas (Benninga et al., 2022; Qiu et al., 2019).

Results varied strongly from field to field, e.g. RMSE values ranged from 0.05 m^3/m^3 to 0.16 m^3/m^3. These rather high variability was also encountered in other studies (Attarzadeh et al., 2018), and might be caused by local conditions related to soil (texture, stoniness, etc.) or crop characteristics (Ouaadi et al., 2020), as well as to the general SM dynamics during the agricultural season on each field.

The analysis of the performance of the methods based on the actual SM conditions showed that highest errors were obtained in dry conditions. SM heterogeneity is known to be higher in dry conditions (Hupet and Vanclooster, 2002), and this might influence both the performance of retrieval techniques and the representativity of field measurements in these conditions. Wet conditions also lead to quite high errors, although not as high as in the dry case. Holtgrave et al. (2018) obtained higher errors for wet conditions with a SVR model and Zhu et al. (2022) with the STCD. These authors interpreted the poor performance for wet conditions as a consequence of the lower sensitivity of SAR backscatter to high SM values. Intermediate SM conditions produced the best performance metrics.

SM retrieval at the field-scale is challenging due to the high complexity of the SAR signal (Bauer-Marschallinger et al., 2019), especially in vegetated areas. Although none of the approaches analyzed in this study achieved the target accuracy threshold of ubRMSE ≤ 0.04 m^3/m^3 defined for low resolution missions (SMOS or SMAP) (Gruber et al., 2020), the use of these SM products could still be useful even with biases (Entekhabi et al., 2010b), as long as the estimations reproduce reasonably the temporal dynamics of SM (Koster et al., 2009). Furthermore, performance metrics have to be interpreted considering that the accuracy of in situ SM probes after detailed laboratory calibrations are at best RMSE ~0.02 m^3/m^3 (Kizito et al., 2008), and RMSE ≥ 0.035 m^3/m^3 are typical in real soil conditions (Kim et al., 2020; Varble and Chávez, 2011), with even higher errors reported for near-surface layers, where RMSE values > 0.1 m^3/m^3 can be obtained (Mittelbach et al., 2012). Furthermore, measurement uncertainty strongly increases with extent scale (Famiglietti et al., 2008).

Finally, the choice of one technique or another is not straightforward, as their performance has been found to be similar. The use of STCD could be more advantageous as it might not need any vegetation correction. However, STCD performance depends on the selection of SM bounds. TUWCD is simple but its accuracy depends on correcting for vegetation effects in backscatter and setting adequate dry and wet bounds. MTBCD is technically more complex, as it requires a preliminary implementation of the IEM. A limitation of this study might be the lack of ground SM data during the summer-autumn period. Further studies focused on this period might complement the results obtained here. In addition, it would be convenient to perform similar analyses elsewhere.

5. Conclusions

In this study, three different SM estimation approaches (STCD, TUWCD and MTBCD) based on Sentinel-1 data were evaluated at the agricultural field scale, showing similar performance metrics between the estimated and measured SM (ubRMSE 7−8 m^3/m^3). In general, higher errors were observed for dry conditions (SM < 0.15 m^3/m^3) where a positive bias was generally observed, particularly for TUWCD. This caused a lower accuracy in late spring months, particularly in rainfed conditions. TUWCD and MTBCD obtained better results after applying a vegetation correction to Sentinel-1 data, conversely for STCD vegetation correction only resulted in minor improvements in SM estimations. From the methodological point of view, it should be noted that STCD provided the best results when applied to rather short time windows (four S-1 observations or ~1 month) and considering rather extreme boundary conditions. TUWCD required setting dry and wet backscatter bounds (which is challenging on agricultural areas subject to crop rotation), this was accomplished by means of a regional and multiyear characterization of wheat fields backscatter statistics. MTBCD required a calibration based on IEM simulations that had to be optimized. Overall, the performance of the evaluated techniques was comparable to similar studies, yet it might be emphasized that in this study they were applied at the agricultural field scale (1–8 ha). Therefore, results were considered promising for the future application of these techniques in irrigation management. It is recommended that similar validation studies be carried out in other locations and conditions to complement the results obtained here.

Funding

This work was supported by the Spanish Ministry of Science and Innovation and the European Regional Development Fund (MICINN/FEDER-UE) through projects [CGL2016–75217-R and PID2019–107386RB-I00 / AEI / 10.13039/501100011033] and doctoral grant [BES-2017–080560].

CRediT authorship contribution statement

María Arias: Data curation, Formal analysis, Investigation, Methodology, Software, Visualization, Writing – original draft. **Claudia Notarnicola:** Methodology, Supervision, Writing – review & editing. **Miguel Ángel Campo-Bescós:** Supervision, Writing – review & editing. **Luis Miguel Arregui:** Data curation. **Jesús Álvarez-Mozos:** Conceptualization, Funding acquisition, Investigation, Methodology, Project administration, Resources, Supervision, Writing – review & editing.

Declaration of Competing Interest

The authors declare the following financial interests/personal relationships which may be considered as potential competing interests: Jesús Álvarez-Mozos reports financial support was provided by Spainish Ministry of Science and Innovation. María Arias reports financial support was provided by Spainish Ministry of Science and Innovation.

Acknowledgements

The authors would like to acknowledge the Government of Navarre for providing the (CAP) declarations database used in this research.

Open access funding provided by the Public University of Navarre.

Appendix A. Supporting information

Supplementary data associated with this article can be found in the online version at doi:10.1016/j.agwat.2023.108422.

References

Al-Khaldi, M.M., Johnson, J.T., O'Brien, A.J., Balenzano, A., Mattia, F., 2019. Time-series retrieval of soil moisture using CYGNSS. IEEE Trans. Geosci. Remote Sens. 57, 4322–4331. https://doi.org/10.1109/TGRS.2018.2890646.

Amazirh, A., Merlin, O., Er-Raki, S., Gao, Q., Rivalland, V., Malbeteau, Y., Khabba, S., Escorihuela, M.J., 2018. Retrieving surface soil moisture at high spatio-temporal resolution from a synergy between Sentinel-1 radar and Landsat thermal data: a study case over bare soil. Remote Sens. Environ. 211, 321–337. https://doi.org/10.1016/j.rse.2018.04.013.

Arias, M., Campo-Bescós, M.A., Alvarez-Mozos, J., 2020. Crop classification based on temporal signatures of sentinel-1 observations over Navarre Province, Spain. Remote Sens 1–29. https://doi.org/10.3390/rs12020278.

Arias, M., Campo-Bescós, M.Á., Álvarez-Mozos, J., 2022a. On the influence of acquisition geometry in backscatter time series over wheat. Int. J. Appl. Earth Obs. Geoinf. 106, 102671 https://doi.org/10.1016/j.jag.2021.102671.

Arias, M., Campo-Bescos, M.A., Arregui, L.M., Gonzalez-Audicana, M., Alvarez-Mozos, J., 2022b. A new methodology for wheat attenuation correction at C-band VV-Polarized Backscatter Time Series. IEEE Trans. Geosci. Remote Sens 60. https://doi.org/10.1109/TGRS.2022.3176144.

Attarzadeh, R., Amini, J., Notarnicola, C., Greifeneder, F., 2018. Synergetic use of Sentinel-1 and Sentinel-2 data for soil moisture mapping at plot scale. Remote Sens 10, 1–18. https://doi.org/10.3390/rs10081285.

Attema, E.P.W., Ulaby, F.T., 1978. Vegetation modeled as a water cloud. Radio Sci. 13, 357–364. https://doi.org/10.1029/RS013i002p00357.

Baghdadi, N., Cresson, R., El Hajj, M., Ludwig, R., La Jeunesse, I., 2012. Estimation of soil parameters over bare agriculture areas from C-band polarimetric SAR data using neural networks. Hydrol. Earth Syst. Sci. 16, 1607–1621. https://doi.org/10.5194/hess-16-1607-2012.

Balenzano, A., Mattia, F., Satalino, G., Davidson, M.W.J., 2011. Dense temporal series of C-band SAR data for soil moisture retrieval over agricultural sites. IEEE J. Sel. Top. Appl. Earth Obs. Remote Sens 4, 439–450. https://doi.org/10.1109/JSTARS.2010.2052916.

Balenzano, A., Satalino, G., Lovergine, F., Rinaldi, M., Iacobellis, V., Mastronardi, N., Mattia, F., 2013. On the use of temporal series of L- and X-band SAR data for soil moisture retrieval. Capitanata plain case study. Eur. J. Remote Sens 46, 721–737. https://doi.org/10.5721/EuJRS20134643.

Balenzano, A., Mattia, F., Satalino, G., Lovergine, F.P., Palmisano, D., Peng, J., Marzahn, P., Wegmüller, U., Cartus, O., Dąbrowska-Zielińska, K., Musial, J.P., Davidson, M.W.J., Pauwels, V.R.N., Cosh, M.H., McNairn, H., Johnson, J.T., Walker, J.P., Yueh, S.H., Entekhabi, D., Kerr, Y.H., Jackson, T.J., 2021. Sentinel-1 soil moisture at 1 km resolution: a validation study. Remote Sens. Environ. 263. https://doi.org/10.1016/j.rse.2021.112554.

Bauer-Marschallinger, B., Freeman, V., Cao, S., Paulik, C., Schaufler, S., Stachl, T., Modanesi, S., Massari, C., Ciabatta, L., Brocca, L., Wagner, W., 2019. Toward Global Soil Moisture Monitoring with Sentinel-1: Harnessing Assets and Overcoming Obstacles. IEEE Trans. Geosci. Remote Sens. 57, 520–539. https://doi.org/10.1109/TGRS.2018.2858004.

Benninga, H.J.F., van der Velde, R., Su, Z., 2022. Soil moisture content retrieval over meadows from Sentinel-1 and Sentinel-2 data using physically based scattering models. Remote Sens. Environ. 280, 113191 https://doi.org/10.1016/j.rse.2022.113191.

Benninga, H.-J.F., van der Velde, R., Su, Z., 2020. Sentinel-1 soil moisture content and its uncertainty over sparsely vegetated fields. J. Hydrol. X 9, 100066. https://doi.org/10.1016/j.hydroa.2020.100066.

Bindlish, R., Barros, A.P., 2001. Parameterization of vegetation backscatter in radar-based, soil moisture estimation. Remote Sens. Environ. 76, 130–137. https://doi.org/10.1016/S0034-4257(00)00200-5.

Brocca, L., Hasenauer, S., Lacava, T., Melone, F., Moramarco, T., Wagner, W., Dorigo, W., Matgen, P., Martínez-Fernández, J., Llorens, P., Latron, J., Martin, C., Bittelli, M., 2011. Soil moisture estimation through ASCAT and AMSR-E sensors: An intercomparison and validation study across Europe. Remote Sens. Environ. 115, 3390–3408. https://doi.org/10.1016/j.rse.2011.08.003.

Brocca, L., Tarpanelli, A., Filippucci, P., Dorigo, W., Zaussinger, F., Gruber, A., Fernández-Prieto, D., 2018. How much water is used for irrigation? A new approach exploiting coarse resolution satellite soil moisture products. Int. J. Appl. Earth Obs. Geoinf. 73, 752–766. https://doi.org/10.1016/j.jag.2018.08.023.

Carranza, C., Benninga, H., van der Velde, R., van der Ploeg, M., 2019. Monitoring agricultural field trafficability using Sentinel-1. Agric. Water Manag 224, 105698. https://doi.org/10.1016/j.agwat.2019.105698.

Chan, S.K., Bindlish, R., O'Neill, P.E., Njoku, E., Jackson, T., Colliander, A., Chen, F., Burgin, M., Dunbar, S., Piepmeier, J., Yueh, S., Entekhabi, D., Cosh, M.H., Caldwell, T., Walker, J., Wu, X., Berg, A., Rowlandson, T., Pacheco, A., McNairn, H., Thibeault, M., Martinez-Fernandez, J., Gonzalez-Zamora, A., Seyfried, M., Bosch, D., Starks, P., Goodrich, D., Prueger, J., Palecki, M., Small, E.E., Zreda, M., Calvet, J.-C., Crow, W.T., Kerr, Y., 2016. Assessment of the SMAP Passive Soil Moisture Product. IEEE Trans. Geosci. Remote Sens 54, 4994–5007. https://doi.org/10.1109/TGRS.2016.2561938.

Dorigo, W., Wagner, W., Albergel, C., Albrecht, F., Balsamo, G., Brocca, L., Chung, D., Ertl, M., Forkel, M., Gruber, A., Haas, E., Hamer, P.D., Hirschi, M., Ikonen, J., de Jeu, R., Kidd, R., Lahoz, W., Liu, Y.Y., Miralles, D., Mistelbauer, T., Nicolai-Shaw, N., Parinussa, R., Pratola, C., Reimer, C., van der Schalie, R., Seneviratne, S.I., Smolander, T., Lecomte, P., 2017. ESA CCI Soil Moisture for improved Earth system understanding: State-of-the art and future directions. Remote Sens. Environ. 203, 185–215. https://doi.org/10.1016/j.rse.2017.07.001.

Dubois, P.C., vanZyl, J., Engman, T., 1995. Corrections to "Measuring Soil Moisture with Imaging Radars. IEEE Trans. Geosci. Remote Sens. 33, 1340. https://doi.org/10.1109/TGRS.1995.477194.

Entekhabi, D., Njoku, E.G., O'Neill, P.E., Kellogg, K.H., Crow, W.T., Edelstein, W.N., Entin, J.K., Goodman, S.D., Jackson, T.J., Johnson, J., Kimball, J., Piepmeier, J.R., Koster, R.D., Martin, N., McDonald, K.C., Moghaddam, M., Moran, S., Reichle, R., Shi, J.C., Spencer, M.W., Thurman, S.W., Tsang, L., Van Zyl, J., 2010a. The Soil Moisture Active Passive (SMAP) Mission. Proc. IEEE 98, 704–716. https://doi.org/10.1109/JPROC.2010.2043918.

Entekhabi, D., Reichle, R.H., Koster, R.D., Crow, W.T., 2010b. Performance metrics for soil moisture retrievals and application requirements. J. Hydrometeorol. 11, 832–840. https://doi.org/10.1175/2010JHM1223.1.

European Commission, 2022. List of potential agricultural practices that eco-schemes could support. European Commission, Directorate-General for Agriculture and Rural Development.

Famiglietti, J.S., Ryu, D., Berg, A.A., Rodell, M., Jackson, T.J., 2008. Field observations of soil moisture variability across scales. Water Resour. Res 44, W01423. https://doi.org/10.1029/2006WR005804.

Fung, A.K., 1994. Microwave Scattering and Emission Models and their Applications. Artech House Publishers.

Gao, Q., Zribi, M., Escorihuela, M., Baghdadi, N., Segui, P., 2018. Irrigation Mapping Using Sentinel-1 Time Series at Field Scale. Remote Sens 10, 1495. https://doi.org/10.3390/rs10091495.

Gelman, A., Carlin, J.B., Stern, H.S., Dunson, D.B., Vehtari, A., Rubin, D.B., 2013. Bayesian Data Analysis, 0 ed. Chapman and Hall/CRC. ⟨https://doi.org/10.1201/b16018⟩.

Green, J.K., Seneviratne, S.I., Berg, A.M., Findell, K.L., Hagemann, S., Lawrence, D.M., Gentine, P., 2019. Large influence of soil moisture on long-term terrestrial carbon uptake. Nature 565, 476–479. https://doi.org/10.1038/s41586-018-0848-x.

Gruber, A., De Lannoy, G., Albergel, C., Al-Yaari, A., Brocca, L., Calvet, J.-C., Colliander, A., Cosh, M., Crow, W., Dorigo, W., Draper, C., Hirschi, M., Kerr, Y., Konings, A., Lahoz, W., McColl, K., Montzka, C., Muñoz-Sabater, J., Peng, J., Reichle, R., Richaume, P., Rüdiger, C., Scanlon, T., van der Schalie, R., Wigneron, J.-P., Wagner, W., 2020. Validation practices for satellite soil moisture retrievals: What are (the) errors. Remote Sens. Environ. 244, 111806 https://doi.org/10.1016/j.rse.2020.111806.

Hallikainen, M.T., Ulabz, F.T., Dobson, M.C., El-Rayes, M.A., Wu, L.K., 1985. Microwave Dielectric Behavior of Wet Soil-Part I: Empirical Models and Experimental Observations. IEEE Trans. Geosci. Remote Sens. GE 23, 25–34. https://doi.org/10.1109/TGRS.1985.289497.

He, L., Qin, Q., Panciera, R., Tanase, M., Walker, J.P., Hong, Y., 2017. An extension of the alpha approximation method for soil moisture estimation using time-series sar data over bare soil surfaces. IEEE Geosci. Remote Sens. Lett. 14, 1328–1332. https://doi.org/10.1109/LGRS.2017.2711006.

Holtgrave, A.K., Förster, M., Greifeneder, F., Notarnicola, C., Kleinschmit, B., 2018. Estimation of Soil Moisture in Vegetation-Covered Floodplains with Sentinel-1 SAR Data Using Support Vector Regression. PFG - J. Photogramm. Remote Sens. Geoinf. Sci. 86, 85–101. https://doi.org/10.1007/s41064-018-0045-4.

Hornáček, M., Wagner, W., Sabel, D., Truong, H.L., Snoeij, P., Hahmann, T., Diedrich, E., Doubková, M., 2012. Potential for high resolution systematic global surface soil moisture retrieval via change detection using sentinel-1. IEEE J. Sel. Top. Appl. Earth Obs. Remote Sens. 5, 1303–1311. https://doi.org/10.1109/JSTARS.2012.2190136.

Hupet, F., Vanclooster, M., 2002. Intraseasonal dynamics of soil moisture variability within a small agricultural maize cropped field. J. Hydrol. 261, 86–101. https://doi.org/10.1016/S0022-1694(02)00016-1.

Kerr, Y.H., Waldteufel, P., Wigneron, J.-P., Martinuzzi, J., Font, J., Berger, M., 2001. Soil moisture retrieval from space: the Soil Moisture and Ocean Salinity (SMOS) mission. IEEE Trans. Geosci. Remote Sens. 39, 1729–1735. https://doi.org/10.1109/36.942551.

Kerr, Y.H., Waldteufel, P., Richaume, P., Wigneron, J.P., Ferrazzoli, P., Mahmoodi, A., Al Bitar, A., Cabot, F., Gruhier, C., Juglea, S.E., Leroux, D., Mialon, A., Delwart, S., 2012. The SMOS Soil Moisture Retrieval Algorithm. IEEE Trans. Geosci. Remote Sens. 50, 1384–1403. https://doi.org/10.1109/TGRS.2012.2184548.

Kim, H., Cosh, M.H., Bindlish, R., Lakshmi, V., 2020. Field evaluation of portable soil water content sensors in a sandy loam. Vadose Zone J. 19, e20033 https://doi.org/10.1002/vzj2.20033.

Kizito, F., Campbell, C.S., Campbell, G.S., Cobos, D.R., Teare, B.L., Carter, B., Hopmans, J.W., 2008. Frequency, electrical conductivity and temperature analysis of a low-cost capacitance soil moisture sensor. J. Hydrol. 352, 367–378. https://doi.org/10.1016/j.jhydrol.2008.01.021.

Koster, R.D., Guo, Z., Yang, R., Dirmeyer, P.A., Mitchell, K., Puma, M.J., 2009. On the nature of soil moisture in land surface models. J. Clim. 22, 4322–4335. https://doi.org/10.1175/2009JCLI2832.1.

Le Page, M., Jarlan, L., El Hajj, M.M., Zribi, M., Baghdadi, N., Boone, A., 2020. Potential for the Detection of Irrigation Events on Maize Plots Using Sentinel-1 Soil Moisture Products. Remote Sens 12, 1621. https://doi.org/10.3390/rs12101621.

Lesiv, M., Laso Bayas, J.C., See, L., Duerauer, M., Dahlia, D., Durando, N., Hazarika, R., Kumar Sahariah, P., Vakolyuk, M., Blyshchyk, V., Bilous, A., Perez-Hoyos, A., Gengler, S., Prestele, R., Bilous, S., Akhtar, I., Ul, H., Singha, K., Choudhury, S.B., Chetri, T., Malek, Ż., Bungnamei, K., Saikia, A., Sahariah, D., Narzary, W., Danylo, O., Sturn, T., Karner, M., McCallum, I., Schepaschenko, D., Moltchanova, E., Fraisl, D., Moorthy, I., Fritz, S., 2019. Estimating the global distribution of field size using crowdsourcing. Glob. Change Biol. 25, 174–186. https://doi.org/10.1111/gcb.14492.

Liu, L., Gudmundsson, L., Hauser, M., Qin, D., Li, S., Seneviratne, S.I., 2020. Soil moisture dominates dryness stress on ecosystem production globally. Nat. Commun. 11, 4892. https://doi.org/10.1038/s41467-020-18631-1.

Liu, Y., Qian, J., Yue, H., 2021. Combined Sentinel-1A With Sentinel-2A to Estimate Soil Moisture in Farmland. IEEE J. Sel. Top. Appl. Earth Obs. Remote Sens. 14, 1292–1310. https://doi.org/10.1109/JSTARS.2020.3043628.

Climate Change and Food Security. In: Lobell, D., Burke, M. (Eds.), 2010. Advances in Global Change Research. Springer, Netherlands, Dordrecht. https://doi.org/10.1007/978-90-481-2953-9.

Ma, C., Li, X., McCabe, M.F., 2020. Retrieval of high-resolution soil moisture through combination of Sentinel-1 and Sentinel-2 data. Remote Sens 12, 1–28. https://doi.org/10.3390/rs12142303.

Mittelbach, H., Lehner, I., Seneviratne, S.I., 2012. Comparison of four soil moisture sensor types under field conditions in Switzerland. J. Hydrol. 430–431, 39–49. https://doi.org/10.1016/j.jhydrol.2012.01.041.

Mladenova, I.E., Jackson, T.J., Bindlish, R., Hensley, S., 2013. Incidence angle normalization of radar backscatter data. IEEE Trans. Geosci. Remote Sens. 51, 1791–1804. https://doi.org/10.1109/TGRS.2012.2205264.

Modanesi, S., Massari, C., Bechtold, M., Lievens, H., Tarpanelli, A., Brocca, L., Zappa, L., De Lannoy, G.J.M., 2022. Challenges and benefits of quantifying irrigation through the assimilation of Sentinel-1 backscatter observations into Noah-MP. Hydrol. Earth Syst. Sci. 26, 4685–4706. https://doi.org/10.5194/hess-26-4685-2022.

Naeimi, V., Scipal, K., Bartalis, Z., Hasenauer, S., Wagner, W., 2009. An Improved Soil Moisture Retrieval Algorithm for ERS and METOP Scatterometer Observations. IEEE Trans. Geosci. Remote Sens. 47, 1999–2013. https://doi.org/10.1109/TGRS.2008.2011617.

Notarnicola, C., 2014. A Bayesian change detection approach for retrieval of soil moisture variations under different roughness conditions. IEEE Geosci. Remote Sens. Lett. 11, 414–418. https://doi.org/10.1109/LGRS.2013.2264159.

Notarnicola, C., Angiulli, M., Posa, F., 2006. Use of Radar and Optical Remotely Sensed Data for Soil Moisture Retrieval Over Vegetated Areas. Ieee Trans. Geosci. Remote Sens. 44, 925–935.

Notarnicola, C., Angiulli, M., Posa, F., 2008. Soil Moisture Retrieval From Remotely Sensed Data: Neural Network Approach Versus Bayesian Method. IEEE Trans. Geosci. Remote Sens. 46, 547–557. https://doi.org/10.1109/TGRS.2007.909951.

Oh, Y., Sarabandi, K., Ulaby, F.T., 1992. An empirical model and an inversion technique for radar scattering from bare soil surfaces. IEEE Trans. Geosci. Remote Sens. 30, 370–381. https://doi.org/10.1109/36.134086.

Ouaadi, N., Jarlan, L., Ezzahar, J., Zribi, M., Khabba, S., Bouras, E., Bousbih, S., Frison, P. L., 2020. Monitoring of wheat crops using the backscattering coefficient and the interferometric coherence derived from Sentinel-1 in semi-arid areas. Remote Sens. Environ. 251, 112050 https://doi.org/10.1016/j.rse.2020.112050.

Ouellette, J.D., Johnson, J.T., Balenzano, A., Mattia, F., Satalino, G., Kim, S.B., Dunbar, R.S., Colliander, A., Cosh, M.H., Caldwell, T.G., Walker, J.P., Berg, A.A., 2017. A Time-Series Approach to Estimating Soil Moisture from Vegetated Surfaces Using L-Band Radar Backscatter. IEEE Trans. Geosci. Remote Sens. 55, 3186–3193. https://doi.org/10.1109/TGRS.2017.2663768.

Palmisano, D., Balenzano, A., Satalino, G., Mattia, F., Pierdicca, N., Monti-guarnieri, A., 2018. Sentinel-1 sensitivity to soil moisture at high incidence angle and its impact on retrieval. Int. Geosci. Remote Sens. Symp. . (IGARSS 2018) 1430–1433.

Pasolli, L., Member, S., Notarnicola, C., Bruzzone, L., 2011. Estimating Soil Moisture With the Support Vector Regression Technique. IEEE Geosci. Remote Sens. Lett. 8, 1080–1084.

Peng, J., Albergel, C., Balenzano, A., Brocca, L., Cartus, O., Cosh, M.H., Crow, W.T., Dabrowska-Zielinska, K., Dadson, S., Davidson, M.W.J., de Rosnay, P., Dorigo, W., Gruber, A., Hagemann, S., Hirschi, M., Kerr, Y.H., Lovergine, F., Mahecha, M.D., Marzahn, P., Mattia, F., Musial, J.P., Preuschmann, S., Reichle, R.H., Satalino, G., Silgram, M., van Bodegom, P.M., Verhoest, N.E.C., Wagner, W., Walker, J.P., Wegmüller, U., Loew, A., 2021. A roadmap for high-resolution satellite soil moisture applications – confronting product characteristics with user requirements. Remote Sens. Environ. 252, 112162 https://doi.org/10.1016/j.rse.2020.112162.

Pulvirenti, L., Squicciarino, G., Cenci, L., Boni, G., Pierdicca, N., Chini, M., Versace, C., Campanella, P., 2018. A surface soil moisture mapping service at national (Italian) scale based on Sentinel-1 data. Environ. Model. Softw. 102, 13–28. https://doi.org/10.1016/j.envsoft.2017.12.022.

Qiu, J., Crow, W.T., Wagner, W., Zhao, T., 2019. Effect of vegetation index choice on soil moisture retrievals via the synergistic use of synthetic aperture radar and optical remote sensing. Int. J. Appl. Earth Obs. Geoinf. 80, 47–57. https://doi.org/10.1016/j.jag.2019.03.015.

Rawls, W.J., Brakensiek, D.L., Saxtonn, K.E., 1982. Estimation of Soil Water Properties. Trans. ASAE 25, 1316–1320. https://doi.org/10.13031/2013.33720.

Saxton, K.E., Rawls, W.J., 2006. Soil Water Characteristic Estimates by Texture and Organic Matter for Hydrologic Solutions. Soil Sci. Soc. Am. J. 70, 1569–1578. https://doi.org/10.2136/sssaj2005.0117.

Seneviratne, S.I., Corti, T., Davin, E.L., Hirschi, M., Jaeger, E.B., Lehner, I., Orlowsky, B., Teuling, A.J., 2010. Investigating soil moisture–climate interactions in a changing climate: A review. Earth-Sci. Rev. 99, 125–161. https://doi.org/10.1016/j.earscirev.2010.02.004.

Shi, H., Lopez-Sanchez, J.M., Yang, J., Li, P., Zhao, L., Zhao, J., 2021. Contribution of Polarimetry and Multi-Incidence to Soil Moisture Estimation over Agricultural Fields Based on Time Series of L-Band SAR Data. IEEE J. Sel. Top. Appl. Earth Obs. Remote Sens 14, 300–313. https://doi.org/10.1109/JSTARS.2020.3036732.

Shi, J., Wang, J., Hsu, A.Y., O'Neill, P.E., Engman, E.T., 1997. Estimation of bare surface soil moisture and surface roughness parameter using L-band SAR image data. IEEE Trans. Geosci. Remote Sens. 35, 1254–1266. https://doi.org/10.1109/36.628792.

Torres, R., Snoeij, P., Geudtner, D., Bibby, D., Davidson, M., Attema, E., Potin, P., Rommen, B., Floury, N., Brown, M., Traver, I.N., Deghaye, P., Duesmann, B., Rosich, B., Miranda, N., Bruno, C., L'Abbate, M., Croci, R., Pietropaolo, A., Huchler, M., Rostan, F., 2012. GMES Sentinel-1 mission. Remote Sens. Environ. 120, 9–24. https://doi.org/10.1016/j.rse.2011.05.028.

Ulaby, F.T., Long, D.G., 2014. Microwave radar and radiometric remote sensing. The University of Michigan Press, Ann Arbor.

Ulaby, F.T., Dubois, P.C., Van Zyl, J., 1996. Radar mapping of surface soil moisture. J. Hydrol. 184, 57–84. https://doi.org/10.1016/0022-1694(95)02968-0.

Varble, J.L., Chávez, J.L., 2011. Performance evaluation and calibration of soil water content and potential sensors for agricultural soils in eastern Colorado. Agric. Water Manag 101, 93–106. https://doi.org/10.1016/j.agwat.2011.09.007.

Veloso, A., Mermoz, S., Bouvet, A., Le Toan, T., Planells, M., Dejoux, J.-F., Ceschia, E., 2017. Understanding the temporal behavior of crops using Sentinel-1 and Sentinel-2-like data for agricultural applications. Remote Sens. Environ. 199, 415–426. https://doi.org/10.1016/j.rse.2017.07.015.

Verhoest, N., Lievens, H., Wagner, W., Álvarez-Mozos, J., Moran, M., Mattia, F., 2008. On the Soil Roughness Parameterization Problem in Soil Moisture Retrieval of Bare Surfaces from Synthetic Aperture Radar. Sensors 8, 4213–4248. https://doi.org/10.3390/s8074213.

Verstraeten, W.W., Veroustraete, F., van der Sande, C.J., Grootaers, I., Feyen, J., 2006. Soil moisture retrieval using thermal inertia, determined with visible and thermal spaceborne data, validated for European forests. Remote Sens. Environ. 101, 299–314. https://doi.org/10.1016/j.rse.2005.12.016.

Wagner, W., Lemoine, G., Rott, H., 1999. A method for estimating soil moisture from ERS Scatterometer and soil data. Remote Sens. Environ. 70, 191–207. https://doi.org/10.1016/S0034-4257(99)00036-X.

Wang, L., Qu, J.J., 2007. NMDI: A normalized multi-band drought index for monitoring soil and vegetation moisture with satellite remote sensing. Geophys. Res. Lett. 34, L20405. https://doi.org/10.1029/2007GL031021.

Wang, Y., Leng, P., Peng, J., Marzahn, P., Ludwig, R., 2021. Global assessments of two blended microwave soil moisture products CCI and SMOS with in-situ measurements and reanalysis data. Int. J. Appl. Earth Obs. Geoinf. 94, 102234 https://doi.org/10.1016/j.jag.2020.102234.

Wasko, C., Nathan, R., 2019. Influence of changes in rainfall and soil moisture on trends in flooding. J. Hydrol. 575, 432–441. https://doi.org/10.1016/j.jhydrol.2019.05.054.

White, E.V., Roy, D.P., 2015. A contemporary decennial examination of changing agricultural field sizes using Landsat time series data: Landsat field size change. Geo Geogr. Environ. 2, 33–54. https://doi.org/10.1002/geo2.4.

Zappa, L., Schlaffer, S., Brocca, L., Vreugdenhil, M., Nendel, C., Dorigo, W., 2022. How accurately can we retrieve irrigation timing and water amounts from (satellite) soil moisture. Int. J. Appl. Earth Obs. Geoinf. 113, 102979 https://doi.org/10.1016/j.jag.2022.102979.

Zeng, J., Li, Z., Chen, Q., Bi, H., Qiu, J., Zou, P., 2015. Evaluation of remotely sensed and reanalysis soil moisture products over the Tibetan Plateau using in-situ observations. Remote Sens. Environ. 163, 91–110. https://doi.org/10.1016/j.rse.2015.03.008.

Zhang, M., Lang, F., Zheng, N., 2021. Soil Moisture Retrieval during the Wheat Growth Cycle Using SAR and Optical Satellite Data. Water 13, 135. https://doi.org/10.3390/w13020135.

Zhang, X., Tang, X., Gao, X., Zhao, H., 2018. Multitemporal Soil Moisture Retrieval over Bare Agricultural Areas by Means of Alpha Model with Multisensor SAR Data. Adv. Meteor. 2018. https://doi.org/10.1155/2018/7914581.

Zhu, L., Si, R., Shen, X., Walker, J.P., 2019. Roughness and vegetation change detection: A pre-processing for soil moisture retrieval from multi-temporal SAR imagery. Remote Sens. Environ. 225, 93–106. https://doi.org/10.1016/j.rse.2019.02.027.

Zhu, L., Si, R., Shen, X., Walker, J.P., 2022. An advanced change detection method for time-series soil moisture retrieval from Sentinel-1. Remote Sens. Environ. 279, 113137 https://doi.org/10.1016/j.rse.2022.113137.

Zhu, L., Yuan, S., Liu, Y., Chen, C., Walker, J.P., 2023. Time series soil moisture retrieval from SAR data: Multi-temporal constraints and a global validation. Remote Sens. Environ. 287, 113466 https://doi.org/10.1016/j.rse.2023.113466.

Zribi, M., Kotti, F., Amri, R., Wagner, W., Shabou, M., Lili-Chabaane, Z., Baghdadi, N., 2014. Soil moisture mapping in a semiarid region, based on ASAR/Wide Swath satellite data. Water Resour. Res. 50, 823–835. https://doi.org/10.1002/2012WR013405.